

ing the pressure recording. Maximal rate of pressure rise ( $dP/dt_{max}$ ) and LV end-diastolic pressure were determined from tracings of LV pressure, and averaged on 100 consecutive cardiac cycles.

**Western blot analysis.** At the age of 13 weeks, three hearts from each group were collected to assess CT-1 expression in the heart. The isolated LV free wall was cut into small pieces and homogenized with a Polytron homogenizer (Kinematica Inc., Cincinnati, Ohio). Homogenates were centrifuged, and the supernatants were collected. For detection of secreted CT-1 from the transferred myoblasts, myoblasts were cultured in DMEM supplemented with 10% FBS, and conditioned media were collected after 72 h incubation. The expression of CT-1 protein was determined by Western blot analysis using an anti-human CT-1 polyclonal antibody (Pepro Tech EC Ltd., London, United Kingdom). The results were quantified by scanning densitometry.

**Histological analysis.** Left ventricular specimens were obtained at the age of 17 weeks ( $n = 5$  for each group). Specimens were frozen with liquid nitrogen and sectioned to 8- $\mu$ m-thick slices. The slices were stained with hematoxylin-eosin. The slices also underwent immunohistochemical staining for skeletal-specific myosin heavy chain by MY-32 monoclonal antibody (Sigma-Aldrich Inc., St. Louis, Missouri), and for CT-1.

In the hematoxylin-eosin-stained sections, the cross-sectional area of cardiac myocytes that was cut transversely and showed nuclei in the center was measured in the free wall and the septum of the LV, respectively. In each side of LV wall, approximately 50 cells were counted per each animal. Before myoblast transplantation, the myocyte size was measured at the age of 6 and 11 weeks ( $n = 5$  for each stage). A total of 100 cells in random areas of LV, including both the free wall and the septum, were counted per each animal, and the average was used for analysis.

**Measurements of plasma angiotensin II (Ang II) and endothelin-1 (ET-1) levels.** At the age of 13 and 17 weeks, blood was collected in a polypropylene tube containing aprotinin (300 kallikrein-inhibiting units/ml) and ethylenediamine-tetraacetic acid (1 mg/ml) and then centrifuged at 3,000 rpm for 15 min at 4°C. The plasma thus obtained was stored at -80°C until assayed. The plasma levels of Ang II and ET-1 were measured by SRL, Inc. (Tokyo, Japan).

**Effects of transferred-gene-derived CT-1 in vitro.** Myoblasts were cultured in DMEM supplemented with 0.1% bovine serum albumin, ITS (10  $\mu$ g/ml insulin, 10  $\mu$ g/ml transferrin, and 10 ng/ml selenious acid), and conditioned media were collected after 72-h incubation. Primary culture of neonatal rat cardiac myocytes was prepared as previously described (21). Cardiac myocytes were treated with either DMEM supplemented with 0.1% bovine serum albumin and ITS (control), the media from myoblasts with or without CT-1-transfer, or 1 nM recombinant human CT-1 (Pepro Tech EC Ltd.) for 48 h. Then cellular

morphology was examined and photographed under light microscopy.

Proliferation and survival tests in myoblasts were performed by use of C2C12 myoblasts (American Type Culture Collection, Manassas, Virginia). Briefly, 5,000 cells were plated in 96-well dishes and grown for 24-h in media containing 10% FBS. The media were then changed to 0% or 10% serum-media, and cell number was determined by the absorbance of the WST-8 reagent (Dojindo Co., Kumamoto, Japan) at 0, 8, 24, and 48 h after media replacement.

**Statistical procedures.** All values were expressed as mean  $\pm$  SEM. The serial measurements of echocardiography were assessed using two-way analysis of variance for repeated measures. The differences at specific stages among groups were analyzed by one-way analysis of variance, followed by Bonferroni's multiple-comparison *t* test. Paired *t* test was used to assess significant differences in myocyte size between areas in each group. Statistical analyses were performed using StatView (version 5.0, SAS Institute Inc., Cary, North Carolina). Values were considered statistically significant at  $p < 0.05$ .

## RESULTS

**Functional assessment after cell transplantation.** The DS rats who were fed a high salt diet developed systemic hypertension ( $>220$  mm Hg) at the age of 11 weeks, which continued until the age of 17 weeks. There was no significant difference in systolic blood pressure among three groups throughout the experiment (Table 1). At the age of 14 to 17 weeks, two rats in the sham group and one rat in the MB group deceased. These animals showed labored respiration with a loss of activity before they died. Therefore, the cause of their death seemed to be congestive heart failure. At the age of 17 weeks, LV end-diastolic pressure increased, and LV  $dP/dt_{max}$  decreased in the sham group, reflecting congestive HF (Table 2). In contrast, LV end-diastolic pressure was not increased, and LV  $dP/dt$  was relatively preserved in both the MB and MB + CT groups. Moreover, LV  $dP/dt_{max}$  was significantly higher in the MB + CT group than in the MB group ( $p < 0.01$ ) (Table 2).

Representative M-mode echocardiograms of the LV at the papillary muscle level were shown in Figure 1A. At the age of 11 weeks, the DS rats developed concentric LV hypertrophy, and there were no differences in preoperative data among the three groups (Fig. 1). At the age of 17 weeks, the sham group showed marked LV dilation and global hypokinesia (Fig. 1A). From the age of 11 to 17 weeks, a marked decrease in %FS and an increase in EDD occurred in sham group, which was associated with a reduction in PWT (%FS,  $50.9 \pm 0.4$  vs.  $32.1 \pm 1.4$ ; EDD,  $5.68 \pm 0.02$  vs.  $7.06 \pm 0.14$  mm; PWT,  $2.12 \pm 0.05$  vs.  $1.68 \pm 0.02$  mm) (Fig. 1B). In contrast, LV dilation was attenuated, and contractile function was maintained significantly in both the MB and MB + CT groups at the age of

**Table 1.** Systolic Blood Pressure and LVW/BW Ratio

	n	SBP (mm Hg)	BW (g)	HW (mg)	LVW (mg)	LVW/BW (mg/g)
Sham						
11 W	7	214 ± 10	333 ± 6			
17 W	3	241 ± 24	337 ± 18	1,468 ± 83	1,221 ± 69	3.7 ± 0.4
MB						
11 W	12	214 ± 8	331 ± 3			
17 W	6	221 ± 13	326 ± 16	1,514 ± 46	1,199 ± 69	3.7 ± 0.1
MB + CT						
11 W	11	201 ± 12	329 ± 5			
17 W	4	233 ± 20	331 ± 5	1,575 ± 32	1,330 ± 30	4.0 ± 0.1

Values are presented as mean ± SEM.

BW = body weight; CT = cardiotrophin; HW = heart weight; LVW = left ventricular weight; MB = myoblasts; SBP = systolic blood pressure; W = the age (weeks).

17 weeks compared with the age-matched sham group (Fig. 1). Moreover, %FS, EDD, and PWT were more preserved in the MB + CT group than in the MB group at the age of 17 weeks (%FS 43.2 ± 0.8 vs. 38.5 ± 1.5; EDD 6.24 ± 0.07 vs. 6.51 ± 0.16 mm; PWT 1.79 ± 0.02 vs. 1.73 ± 0.02 mm, p < 0.05, respectively) (Fig. 1B). On the other hand, B-mode echocardiogram did not exhibit asymmetrical LV wall motion after cell transplantation in both the MB and MB + CT groups (data not shown).

We also performed Holter electrocardiogram in some animals at the age of 17 weeks, which revealed no lethal arrhythmias after cell transplantation (n = 3 in the MB group and n = 2 in the MB + CT group, data not shown).

**Grafted myoblasts in the myocardium.** Serial sections of the transplanted area after cell transplantation were shown in Figure 2. Graft survival was identified at six weeks after transplantation (the age of 17 weeks) by hematoxylin-eosin staining and immunohistochemical staining for skeletal-specific myosin heavy chain, by MY-32 mAb. Multinuclear elongated structure was identified in H-E staining, which indicates that myoblasts had differentiated into myotubes (Fig. 2). These muscular structures were positively stained with MY-32 (Fig. 2), whereas no cells were stained in the PBS-injected hearts. Positive staining for skeletal myosin heavy chain revealed the presence of myotubes. Surviving cells aligned with the cardiac fiber axis within the native myocardium. On the other hand, accumulation of inflammatory cells was hardly detected around the transplanted area at day 0 and two weeks, four weeks, and six weeks after transplantation in both MB and MB + CT groups. As reported previously, the fibrosis was found mainly in

perivascular regions of the arterioles (11), and there were no differences in the extent of fibrosis among the three groups.

**CT-1 expression in the myocardium after cell transplantation.** The secretion of transferred gene-derived CT-1 was confirmed in vitro by Western blot analysis (Fig. 3A). Immunohistochemical staining of the transplanted area for CT-1 is shown in Fig. 3B. Myotubes positively stained for CT-1 were detected in the MB + CT group at six weeks after transplantation, whereas no myotubes were stained in the MB group (Fig. 3B). These data suggest that local expression of CT-1 in CT-1-transfected cells was sustained. Positive staining of myocardium for CT-1, although slightly, was also detected, indicating that endogenous CT-1 was expressed in the myocardium. Western blot analysis revealed that tissue expression of CT-1 in the LV free wall of the MB + CT group significantly increased compared with sham group at two weeks after transplantation (Fig. 3C) (2.3 ± 0.5-fold, p < 0.05).

**Morphometry of the ventricular myocytes.** The cross-sectional area of LV myocytes markedly increased from the age of 6 to 11 weeks (Fig. 4B). Then the sham group exhibited a slight decrease of myocyte size, although statistically not significant, from the age of 11 to 17 weeks (Fig. 4B). In contrast, the myocyte size in both the free wall and the septum wall of LV increased in the MB + CT group, from the age of 11 to 17 weeks (Fig. 4B). At the age of 17 weeks, although no difference in myocyte size was found between the sham and MB groups, the myocyte size in the free wall was 20% larger in the MB + CT group than in sham group (p < 0.05) (Figs. 4A and 4B). Furthermore, the myocyte size in the free wall at the cell-injected site was significantly larger than that of septum wall at the remote site of cell injection in the MB + CT group at this stage (p < 0.05) (Fig. 4B). On the other hand, the myocyte size in the free wall did not significantly differ from that of the septum wall in both the sham and MB groups. We also demonstrated that the conditioned media from CT-1-transferred myoblasts induced cardiac myocyte hypertrophy in vitro (Fig. 4C). These data suggest that CT-1 secreted from grafted cells in the MB + CT group induced hypertrophy of the adjacent myocardial cells in a paracrine manner.

**Table 2.** Hemodynamics at the Age of 17 Weeks

	Sham (n = 4)	MB (n = 6)	MB + CT (n = 7)
dP/dt max, mm Hg/s	887.8 ± 85.2	1,252 ± 35†	1,849 ± 168†‡
LVEDP, mm Hg	14.0 ± 2.9	6.9 ± 2.3*	6.8 ± 1.1*

Values are presented as mean ± SEM. \*p < 0.05 and †p < 0.01 vs. sham group; ‡p < 0.01 vs. MB group by ANOVA and Bonferroni's multiple-comparison t test.

CT = cardiotrophin; dP/dt = maximal dP/dt; LVEDP = Left ventricular end-diastolic pressure; MB = myoblasts.

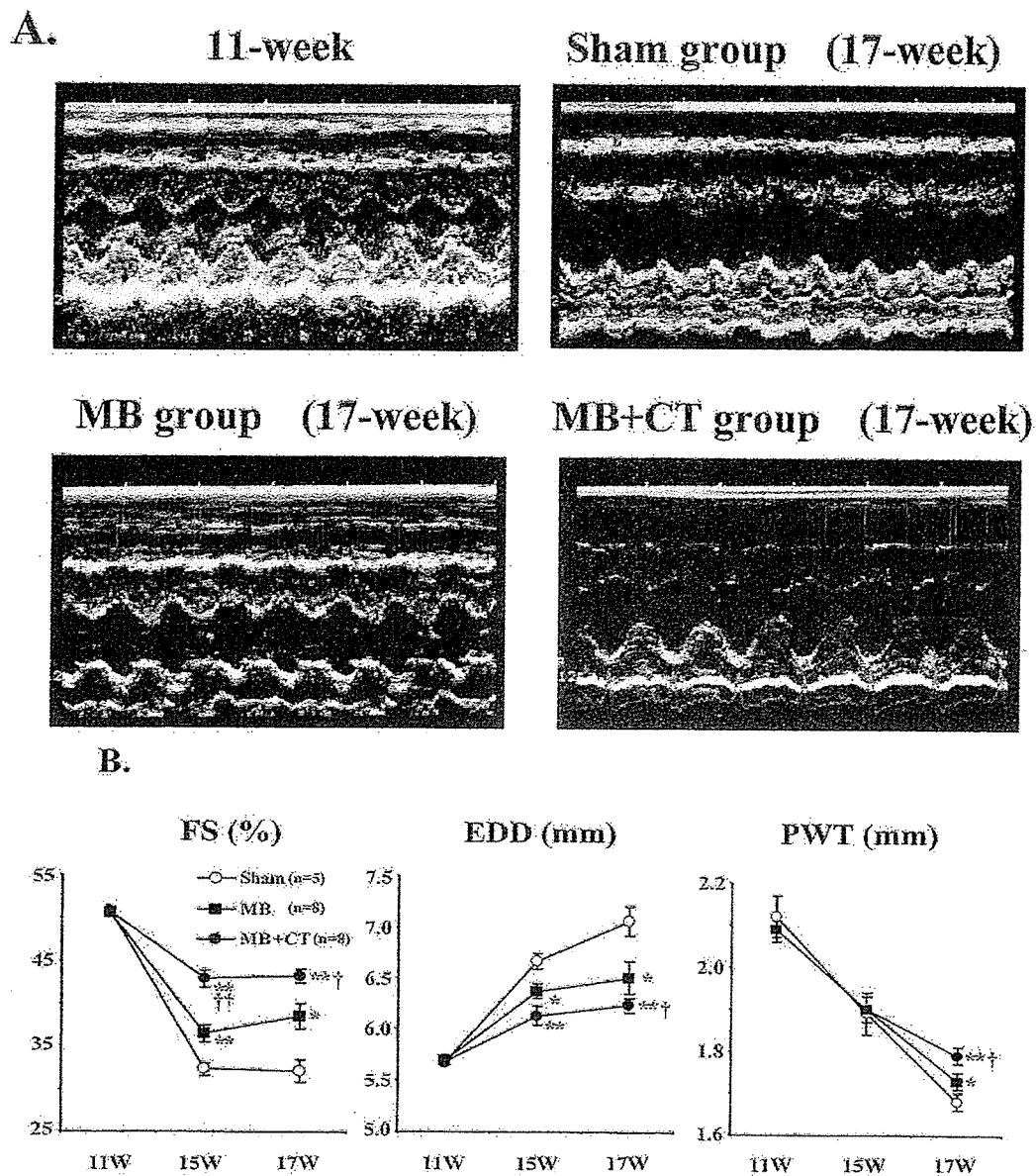


**Figure 1.** (A) Representative tracings of left ventricular M-mode echocardiograms of the sham group at the age of 11 weeks (upper left) and 17 weeks (upper right), the myoblast transplantation (MB) group (lower left), and the transplantation of CT-1-expressing myoblasts (MB + CT) group (lower right) at the age of 17 weeks. Left ventricular dilation and contractile dysfunction were attenuated in both MB and MB + CT groups at the heart failure stage (six weeks after transplantation). (B) Serial measurements of echocardiography in the sham, MB, and MB + CT groups. A p value by two-way analysis of variance: group <0.001; time course <0.001; group/time course interaction <0.001 for each parameter. \*p < 0.05 and \*\*p < 0.01 vs. sham group; †p < 0.05, and ††p < 0.01 vs. MB group at same stage by Bonferroni's multiple-comparison *t* test. Values are means ± SEM. EDD = end-diastolic diameter; FS = fractional shortening; PWT = posterior wall thickness; W = the age (weeks).

**Neurohumoral regulation during the transition to congestive HF.** In this DS rat model, it has been demonstrated that the activation of local renin-angiotensin and endothelin systems in the heart contributes to the transition to heart failure (22,23). Indeed, serum Ang II levels increased at the congestive heart failure stage compared with the LV hypertrophy stage in sham group (Fig. 5A). However, these changes were attenuated in both the MB and MB + CT groups, and the degree of attenuation was greater in MB + CT group than the MB group (p < 0.05) (Fig. 5A). The serum ET-1 levels were also upregulated

during the transition to congestive heart failure in sham group, but remained unchanged in both the MB and MB + CT groups (Fig. 5B). We also found that upregulation of angiotensinogen, angiotensin-converting enzyme, prepro-ET-1, and ET-converting enzyme messenger ribonucleic acid in the LV during the transition to congestive heart failure were all attenuated by myoblast transplantation, using semiquantitative reverse transcriptase-polymerase chain reaction (data not shown).

**The effect of CT-1 on myoblast survival in vitro.** To examine the effect of CT-1 on myoblast survival in vitro, we

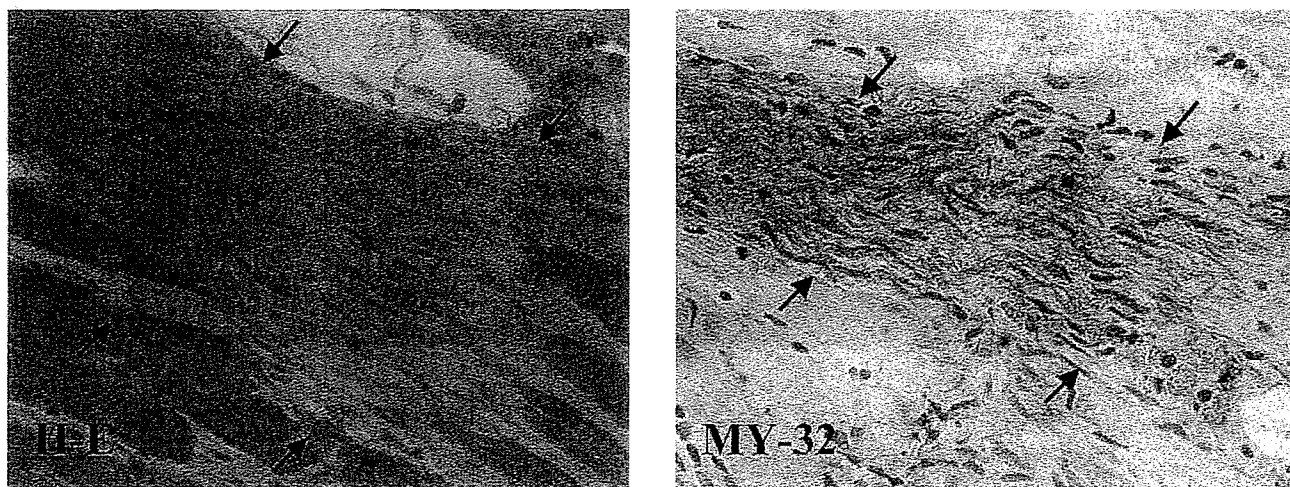


**Figure 2.** Serial sections of transplanted area at the age of 17 weeks (six weeks after transplantation). **Left panel** shows hematoxylin-eosin (H-E) staining. Multinuclear elongated structure is typical of myotubes (arrows). **Right panel** shows immunohistochemical staining for skeletal-specific myosin heavy chain by MY-32. Positive staining with MY-32 demonstrates the presence of myotubes (arrows). Original magnification,  $\times 400$ .

used C2C12 myoblasts rather than rat myoblasts (harvested from rats) to avoid contamination of other type cells such as fibroblasts. Proliferation rates of cells were measured in 10% serum-media. Although statistically not significant, the number of C2C12 cells transferred CT-1 by retrovirus (C2C12<sub>CT-1</sub>) tended to be higher than that of parental C2C12 cells at 48 h (Fig. 6A). Then we assessed whether C2C12<sub>CT-1</sub> cells were resistant to serum-deprivation-induced cell death. In the absence of serum, C2C12 cells rapidly died, whereas C2C12<sub>CT-1</sub> cells not only survived but also proliferated (Fig. 6B). This protective effect was also observed by addition of CT-1 in culture medium (Fig. 6B). Based on these findings, it is likely that CT-1 augments the graft survival ratio in the myocardium.

## DISCUSSION

In the present study, we examined the effect of skeletal myoblast transplantation with and without CT-1 gene transfer on global heart failure of nonischemic cause.

We demonstrated that the transplantation of skeletal myoblasts alleviated the transition from compensatory hypertrophy to congestive heart failure in DS hypertensive rats. So far, only a few animal studies showed that direct intramyocardial injection of fetal cardiac myocytes and smooth muscle cells could improve cardiac function in global heart failure due to nonischemic causes (8–10). Suzuki *et al.* (24) showed the efficient transplantation of skeletal myoblasts via the intracoronary route to doxorubicin-induced HF. Indeed, intracoronary injection is a reasonable method for global dissemination of cells into the heart, but there might be a danger of myocardial infarction. Intramyocardial injection is the most practical method for cell delivery in human patients at the moment. In this study, we injected skeletal myoblasts directly into the myocardium of DS hypertensive rats at the LV hypertrophy stage (the age of 11 weeks).

Six weeks after transplantation, the transplanted myoblasts survived and formed myotubes, which aligned with cardiac fiber axis within the native myocardium.

Echocardiographic examination demonstrated reduced %FS, increased EDD, and decreased PWT at the congestive HF stage (the age of 17 weeks) in all groups. Therefore, ventricular dilation and thinning of the ventricular wall were associated with reduced cardiac contractility. Myocardial muscle fiber slippage and realignment are implicated in the ventricular remodeling of DS hypertensive rats, particularly in the thinning of the myocardium (25). Myoblast transplantation attenuated these morphologic changes associated with ventricular remodeling and served to preserve ventricular function in DS hypertensive rats. Although the precise mechanisms underlying the beneficial effect of myoblast transplantation have not been fully elucidated, it is likely that their passive girdling effect against mechanical stretching prevented LV dilation and remodeling (1). In DS hypertensive rats, activations of local renin-angiotensin or ET systems and matrix metalloproteinases in the heart contribute to LV remodeling and contractile dysfunction during the transition to heart failure (22,23,25). We found that myoblast transplantation attenuated upregulation of renin-angiotensin and ET systems during the transition to congestive HF. Although a causal relationship between the alteration of these neurohumoral regulations and the functional outcome remains elusive, it is possible that a decrease in wall stress due to the elastic property of engrafted cells attenuated the expression of such neurohumoral factors and alleviated the LV remodeling. On the other hand, there is a possibility that inflammation by direct injection induced paracrine effects, such as secretion of growth factors, and improved the cardiac function (8), but accumulation of inflammatory cells was hardly detected around the transplanted area throughout the experiment.

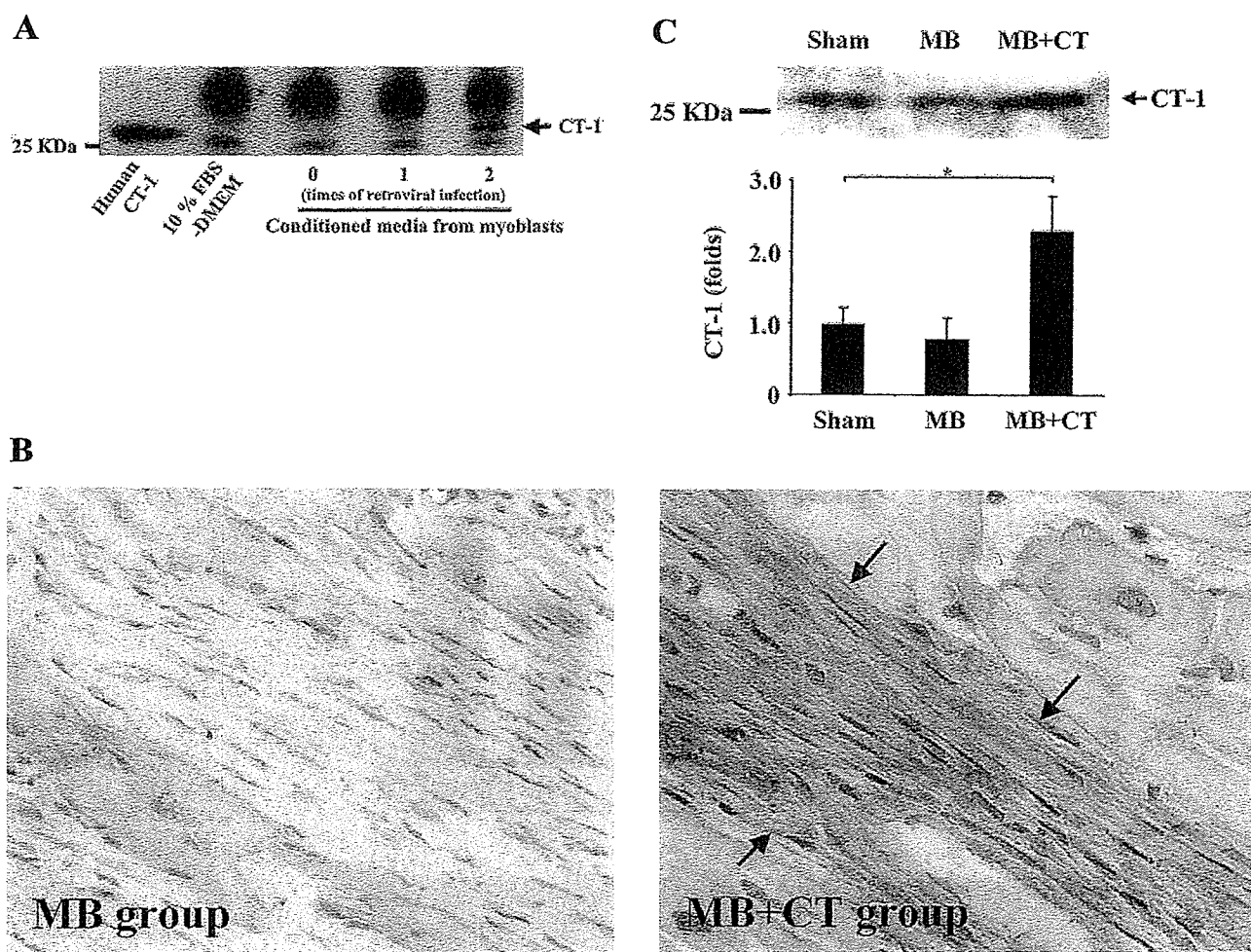


**Figure 3.** (A) Detection of secreted cardiostrophin-1 (CT-1) in culture media by Western blot analysis. Human CT-1 was detected as a 26-kDa band. Only nonspecific staining was seen in 10% FBS-DMEM and the conditioned media from parental myoblasts. In the media from CT-1-transferred myoblasts, CT-1 was detected in addition to nonspecific staining. Twice, infections of retrovirus augmented the CT-1 expression. (B) Transplanted area stained for CT-1 in the myoblast (MB) group (left) and the MB + CT group (right) at the age of 17 weeks (six weeks after transplantation). Grafted cells in the MB + CT group showed positive staining for CT-1 (arrows). Original magnification,  $\times 400$ . (C) Western blot analysis for CT-1 in the left ventricular free wall. Each protein level of CT-1 was normalized to a mean value of sham group ( $n = 5$  for each). \* $p < 0.05$  vs. sham group. Values are means  $\pm$  SEM.

Active force generation by grafted cells is another conceivable mechanism (1). After engraftment, myoblasts merge into myotubes, and this graft might contract in synchrony with the host tissue. Because gap junction proteins, such as N-cadherin and connexin-43, have been shown to be downregulated after differentiation into myotubes, the presence of electromechanical coupling seems unlikely (26,27). On the other hand, simple stretch might initiate contraction of myotubes (28).

The efficiency of the cell-mediated gene delivery, which employs skeletal myoblasts expressing transforming growth factor- $\beta_1$  or vascular endothelial growth factor, has been reported (12,13). We examined the effect of prolonged overexpression of CT-1 in the myocardium by myoblast-mediated gene transfer using retrovirus.

Cardiostrophin-1 has hypertrophic and cardioprotective properties and acts through LIF receptor beta/glycoprotein 130(gp130)-coupled signaling pathway (14-16). Cardiostrophin-

1 promotes cardiac myocyte hypertrophy by directing sarcomere assembly in series in vitro (15). On the other hand, CT-1 prolongs survival of cardiac myocytes (16,29). Cardiac myocyte-restricted knockout of gp130 in adult mice develops LV dilation and induces apoptosis in the myocardium when the LV is subjected to increased wall stress, suggesting that gp130 signaling has the protective effect on cardiac myocytes (30). In chronic HF, CT-1 expression in the myocardium is upregulated corresponding to the severity (17,18). In this study, we demonstrated that the transplantation of skeletal myoblasts expressing CT-1 provides further benefits in preserving cardiac function compared with myoblast transplantation alone, suggesting that CT-1 has the protective effects against ventricular remodeling.

Western blot analysis showed the CT-1 secretion from CT-1-gene transferred myoblasts in vitro and the increased expression of CT-1 in the LV free wall of the MB + CT group in vivo. Immunohistochemical staining exhibited

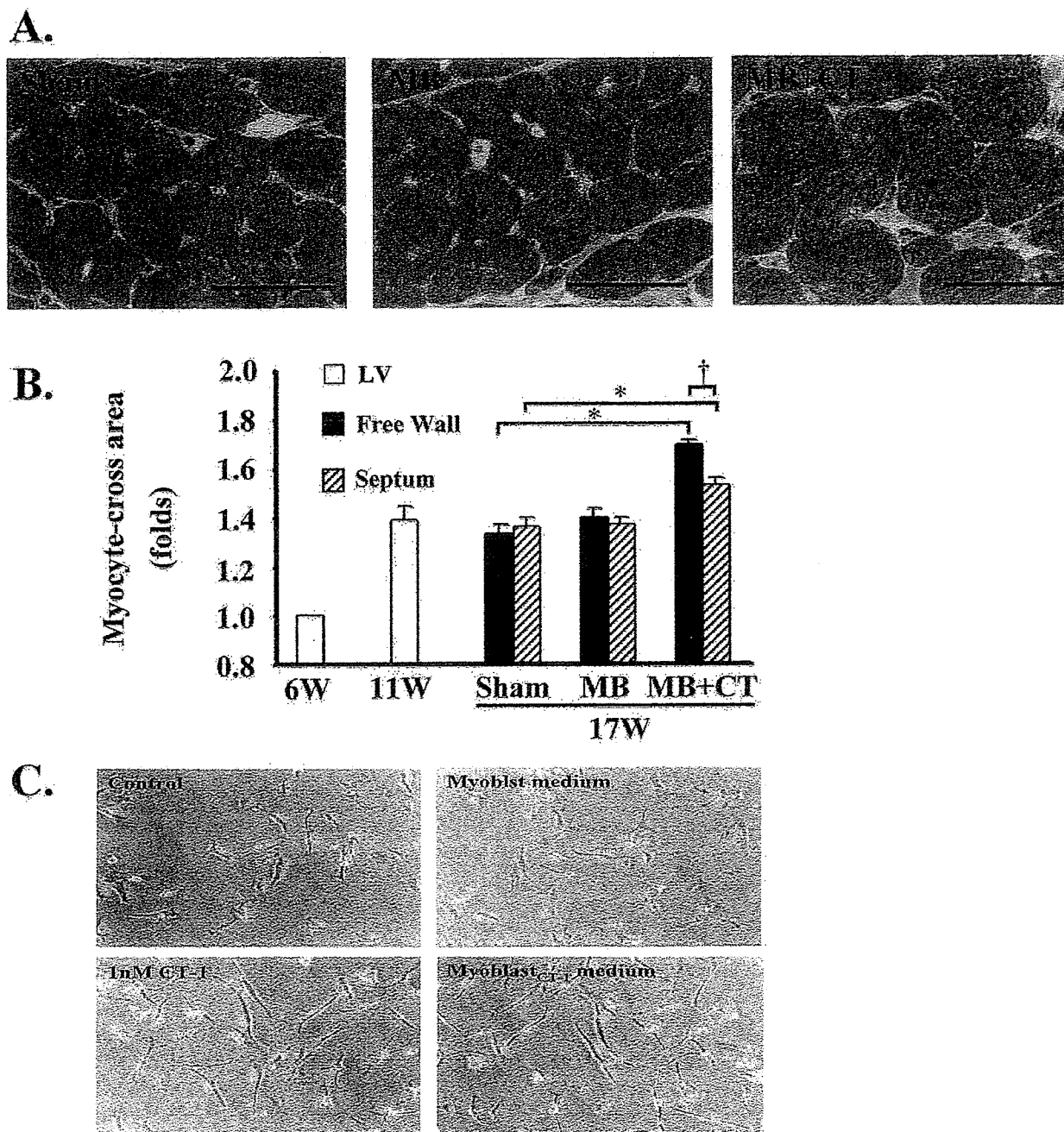


**Figure 4.** (A) Photomicrographs of cardiac myocytes in the anterior aspect of left ventricular (LV) free wall at the age of 17 weeks in sham (left), myoblast (MB) (center), and MB + cardiotrophin (CT) (right) groups. The bar indicates 50  $\mu\text{m}$ . (B) Relative cross-sectional area of cardiac myocytes in the LV (open bars), the free wall (solid bars), and the septum (striped bars) of the LV. Myocyte size was normalized to a mean value of Dahl salt-sensitive rats at the age of six weeks. \* $p < 0.05$  vs. sham group by analysis of variance and Bonferroni's multiple-comparison  $t$  test. † $p < 0.05$  versus the septum wall by paired  $t$  test. Values are means  $\pm$  SEM. (C) Phase-contrast photomicrographs of cultured neonatal rat ventricular cardiac myocytes (CM). Cardiac myocytes were treated as described for 48 h. The media from parental myoblasts showed no morphologic changes compared with control. The media from CT-1-transferred myoblasts induced myocardial cell hypertrophy, similar to that seen in 1 nM CT-1-incubated CMs. Myoblast<sub>CT-1</sub> = CT-1-transferred myoblasts.

that, in the MB + CT group, overexpression of CT-1 in grafted cells within myocardium sustained until six weeks after transplantation. The plasma level of CT-1 was not evaluated in this study. Intravenous injection of CT-1 has been reported to elicit systemic hypotension via a nitric oxide-dependent mechanism (31). Because there were no significant differences in systolic blood pressure among three

groups throughout the experiment, the plasma level of CT-1 was probably not elevated in the MB + CT group compared with the other two groups. We speculate that transferred gene-derived CT-1 operated in an autocrine/paracrine manner at the stage of transition from compensated to decompensated HF.

Transferred gene-derived CT-1 induced myocardial cell

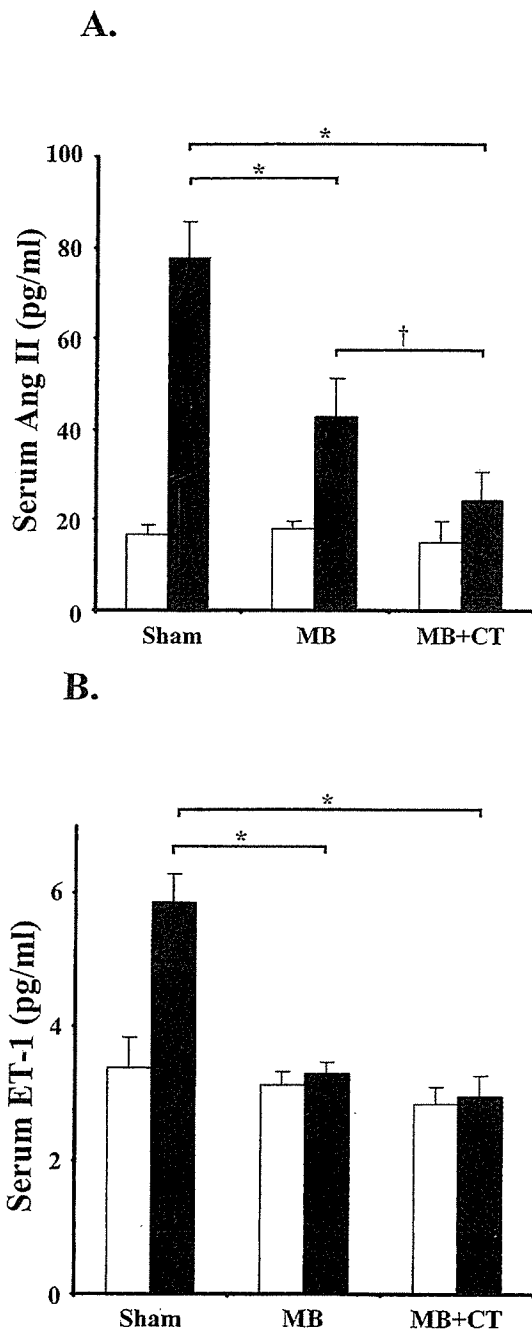


**Figure 5.** Plasma levels of angiotensin II (Ang II) (A) and endothelin-1 (ET-1) (B) at the age of 13 weeks (open bars) and 17 weeks (solid bars). Values are means  $\pm$  SEM.  $n = 5$  per group. \* $p < 0.05$  vs. sham group; † $p < 0.05$  vs. myoblast (MB) group at same stage by analysis of variance and Bonferroni's multiple-comparison  $t$  test. CT = cardiostrophin.

hypertrophy in vitro, and histological examination revealed the increased cross-sectional area of myocytes in the MB + CT group in congestive heart failure stage compared with the MB group. Echocardiographic examination also revealed that the wall thickness was more preserved at the congestive HF stage in the MB + CT group compared with the MB group. Excessive hypertrophy may induce contrac-

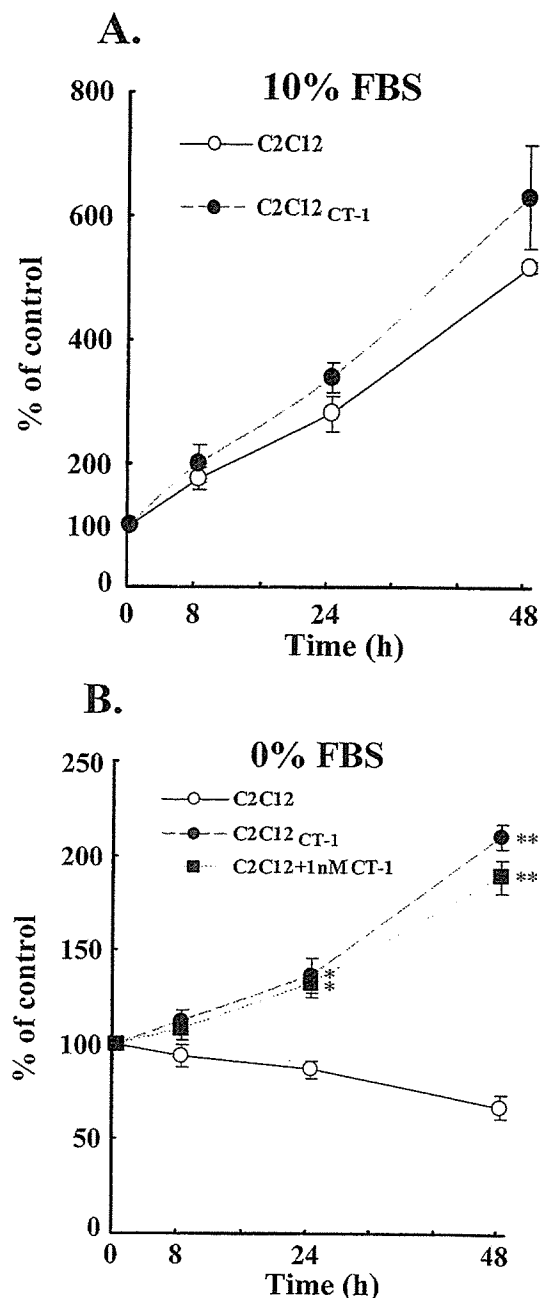


**Figure 6.** Proliferation and survival of parental and cardiostrophin-1 (CT-1)-transferred myoblasts in media containing 10% (A) or 0% (B) serum. Cell number was determined by the absorbance of the WST-8 reagent. Optical density values were normalized to the mean value of each group at 0 h. Data are presented as mean  $\pm$  SEM of four measurements. \* $p < 0.05$  and \*\* $p < 0.01$  vs. parental C2C12 cells at same time point by analysis of variance and Bonferroni's multiple-comparison  $t$  test. C2C12<sub>CT-1</sub> = CT-1-transferred C2C12 cells.

tile dysfunction, but the cardiac function of the MB + CT group was preserved more effectively than the MB groups. Although no definite mechanism has been proven in the relationship between contractile function and myocardial hypertrophy, the present findings suggest that CT-1 from the transplanted cells serves to maintain cardiac function by

inducing hypertrophy of the adjacent cardiac myocytes. Cardiotrophin-1 is known to be a survival factor for cardiac myocytes (16). In the present study, we revealed that CT-1 also has a survival effect on myoblast in vitro. Therefore, it is also possible that CT-1 augmented the graft survival ratio in the myocardium and, thus, enhanced the beneficial effects of cell transplantation. To elucidate this issue, quantitative assessment of the area of injected myoblasts is needed. Also, it is important to verify that myoblasts were injected to the equivalent extent of areas between rats in the MB group and those in the MB + CT group. We tried to measure the graft survival ratio by use of a retroviral vector encoding CT-1-IRES (internal ribosomal entry site)-green fluorescent protein gene; however, the system did not work in the transplanted hearts. Those are the limitations of the present study, and recently reported new methods may help to resolve this issue (32,33).

In conclusion, we demonstrated that MB myoblasts alleviated the transition from compensatory hypertrophy to congestive heart failure in DS hypertensive rats. Transplantation of CT-1-expressing skeletal myoblasts by retroviral-mediated gene transfer resulted in prolonged overexpression of CT-1 within myocardium and preserved cardiac function more effectively. The results of this study suggest that CT-1 has the protective effects against ventricular remodeling. Transplantation of skeletal myoblasts combined with CT-1-gene transfer could be a useful strategy for the treatment of HF.

#### Acknowledgments

The authors are grateful to Ms. Kiyoko Matsui for her skillful technical assistance. Dr. Toh thanks Takami T. for her encouragement.

**Reprint requests and correspondence:** Dr. Seinosuke Kawashima, Division of Cardiovascular and Respiratory Medicine, Department of Internal Medicine, Kobe University Graduate School of Medicine, Kobe, Japan, 7-5-1, Kusunoki-cho, Chuo-ku, Kobe 650-0017, Japan. E-mail: kawashim@med.kobe-u.ac.jp.

#### REFERENCES


- Hagège AA, Vilquin J-T, Bruneval P, Menasché P. Regeneration of the myocardium: a new role in the treatment of ischemic heart disease? *Hypertension* 2001;38:1413-5.
- Taylor DA, Atkins BZ, Hungspreugs P, et al. Regenerating functional myocardium: improved performance after skeletal myoblast transplantation. *Nat Med* 1998;4:929-33.
- Chiu RC-J, Zibaitis A, Kao RL. Cellular cardiomyoplasty: myocardial regeneration with satellite cell implantation. *Ann Thorac Surg* 1995;60:12-8.
- Jain M, DerSimonian H, Brenner DA, et al. Cell therapy attenuates deleterious ventricular remodeling and improves cardiac performance after myocardial infarction. *Circulation* 2001;103:1920-7.
- Pouzet B, Ghostine S, Vilquin J-T, et al. Is skeletal myoblast transplantation clinically relevant in the era of angiotensin-converting enzyme inhibitors? *Circulation* 2001;104 Suppl I:I223-8.
- Menasché P, Hagège AA, Scorsin M, et al. Myoblast transplantation for heart failure. *Lancet* 2001;357:279-80.
- Menasché P, Hagège AA, Vilquin JT, et al. Autologous skeletal myoblast transplantation for severe postinfarction left ventricular dysfunction. *J Am Coll Cardiol* 2003;41:1078-83.
- Scorsin M, Hagège AA, Dolizy I, et al. Can cellular transplantation improve function in doxorubicin-induced heart failure? *Circulation* 1998;98 Suppl III:III51-5.
- Yoo KJ, Li RK, Weisel RD, et al. Heart cell transplantation improves heart function in dilated cardiomyopathic hamsters. *Circulation* 2000;102 Suppl III:III204-9.
- Yoo KJ, Li RK, Weisel RD, et al. Autologous smooth muscle cell transplantation improved heart function in dilated cardiomyopathy. *Ann Thorac Surg* 2000;70:859-65.
- Inoko M, Kihara Y, Morii I, Fujiwara H, Sasayama S. Transition from compensatory hypertrophy to dilated, failing left ventricles in Dahl salt-sensitive rats. *Am J Physiol* 1994;267:H2471-82.
- Suzuki K, Murtuza B, Suzuki N, et al. Cell transplantation for the treatment of acute myocardial infarction using vascular endothelial growth factor-expressing skeletal myoblast. *Circulation* 2001;104 Suppl I:I207-12.
- Koh GY, Kim SJ, Klug MG, et al. Targeted expression of transforming growth factor- $\beta$ 1 in intracardiac grafts promotes vascular endothelial cell DNA synthesis. *J Clin Invest* 1995;95:114-21.
- Pennica D, Swanson TA, Shaw KJ, et al. Human cardiotrophin-1: protein and gene structure, biological and binding activities, and chromosomal localization. *Cytokine* 1996;8:183-9.
- Wollert KC, Taga T, Saito M, et al. Cardiotrophin-1 activates a distinct form of cardiac muscle cell hypertrophy: assembly of sarcomeric units in series via gp130/leukemia inhibitory factor. *J Biol Chem* 1996;271:9535-45.
- Sheng Z, Pennica D, Wood WI, et al. Cardiotrophin-1 displays early expression in the murine heart tube and promotes cardiac myocyte survival. *Development* 1996;122:419-28.
- Jougasaki M, Tachibana I, Luchner A, et al. Augmented cardiac cardiotrophin-1 in experimental congestive heart failure. *Circulation* 2000;101:14-7.
- Tsutamoto T, Wada A, Maeda K, et al. Relationship between plasma level of cardiotrophin-1 and left ventricular mass index in patients with dilated cardiomyopathy. *J Am Coll Cardiol* 2001;38:1485-90.
- Weber E, Anderson WF, Kasahara N. Recent advances in retrovirus vector-mediated gene therapy: teaching an old vector new tricks. *Curr Opin Mol Ther* 2001;3:439-53.
- Malik P, Krall WJ, Yu X, et al. Retroviral-mediated gene expression in human myelomonocytic cells: a comparison of hematopoietic cell promoters to viral promoters. *Blood* 1995;86:2993-3005.
- Ueyama T, Sakoda T, Kawashima S, et al. Activated RhoA stimulates c-fos gene expression in myocardial cells. *Circ Res* 1997;81:672-8.
- Iwanaga Y, Kihara Y, Inagaki K, et al. Differential effects of angiotensin II versus endothelin-1 inhibitions in hypertrophic left ventricular myocardium during transition to heart failure. *Circulation* 2001;104:606-12.
- Sakata Y, Masuyama T, Yamamoto K, et al. Renin-angiotensin system-dependent hypertrophy as a contributor to heart failure in hypertensive rats: different characteristics from renin-angiotensin system-independent hypertrophy. *J Am Coll Cardiol* 2001;37:293-9.
- Suzuki K, Murtuza B, Suzuki N, Smolenski RT, Yacoub MH. Intracoronary infusion of skeletal myoblasts improves cardiac function in doxorubicin-induced heart failure. *Circulation* 2001;104 Suppl I:I213-7.
- Iwanaga Yaoyama T, Kihara Y, Onozawa Y, Yoneda T, Sasayama S. Excessive activation of matrix metalloproteinases coincides with left ventricular remodeling during transition from hypertrophy to heart failure in hypertensive rats. *J Am Coll Cardiol* 2002;39:1384-91.
- Murry CE, Wiseman RW, Schwartz SM, Hauschka SD. Skeletal myoblast transplantation for repair of myocardial necrosis. *J Clin Invest* 1996;98:2512-23.
- Reinecke H, MacDonald GH, Hauschka SD, Murry CE. Electromechanical coupling between skeletal and cardiac muscle: implications for infarct repair. *J Cell Biol* 2000;149:731-40.



28. Hutcheson KA, Atkins BZ, Hueman MT, Hopkins MB, Glower DD, Taylor DA. Comparison of benefits on myocardial performance of cellular cardiomyoplasty with skeletal myoblasts and fibroblasts. *Cell Transplant* 2000;9:359-68.
29. Liao Z, Brar BK, Cai Q, et al. Cardiotrophin-1 (CT-1) can protect the adult heart from injury when added both prior to ischemia and at reperfusion. *Cardiovasc Res* 2002;53:902-10.
30. Hirota H, Chen J, Betz UA, et al. Loss of a gp130 cardiac muscle cell survival pathway is a critical event in the onset of heart failure during biomechanical stress. *Cell* 1999;8:920-6.
31. Hamanaka I, Saito Y, Nishikimi T, et al. Effects of cardiotrophin-1 on hemodynamics and endocrine function of the heart. *Am J Physiol* 2000;279:H388-96.
32. Garot J, Untersee T, Teiger E, et al. Magnetic resonance imaging of targeted catheter-based implantation of myogenic precursor cells into infarcted left ventricular myocardium. *J Am Coll Cardiol* 2003;41:1841-6.
33. Wu JC, Chen IY, Sundaresan G, et al. Molecular imaging of cardiac cell transplantation in living animals using optical bioluminescence and positron emission tomography. *Circulation* 2003;108:1302-5.

# Circulation Research

JOURNAL OF THE AMERICAN HEART ASSOCIATION

American Heart  
Association®   
*Learn and Live*<sup>SM</sup>

## **Stoichiometric Relationships Between Endothelial Tetrahydrobiopterin, Endothelial NO Synthase (eNOS) Activity, and eNOS Coupling in Vivo: Insights From Transgenic Mice With Endothelial-Targeted GTP Cyclohydrolase 1 and eNOS Overexpression**

Jennifer K. Bendall, Nicholas J. Alp, Nicholas Warrick, Shijie Cai, David Adlam, Kirk Rockett, Mitsuhiro Yokoyama, Seinosuke Kawashima and Keith M. Channon  
*Circ. Res.* 2005;97;864-871; originally published online Sep 22, 2005;

DOI: 10.1161/01.RES.0000187447.03525.72

Circulation Research is published by the American Heart Association, 7272 Greenville Avenue, Dallas, TX 75214

Copyright © 2005 American Heart Association. All rights reserved. Print ISSN: 0009-7330. Online ISSN: 1524-4571

The online version of this article, along with updated information and services, is located on the World Wide Web at:  
<http://circres.ahajournals.org/cgi/content/full/97/9/864>

Subscriptions: Information about subscribing to Circulation Research is online at <http://circres.ahajournals.org/subscriptions/>

Permissions: Permissions & Rights Desk, Lippincott Williams & Wilkins, a division of Wolters Kluwer Health, 351 West Camden Street, Baltimore, MD 21202-2436. Phone: 410-528-4050. Fax: 410-528-8550. E-mail: [journalpermissions@lww.com](mailto:journalpermissions@lww.com)

Reprints: Information about reprints can be found online at <http://www.lww.com/reprints>

# Stoichiometric Relationships Between Endothelial Tetrahydrobiopterin, Endothelial NO Synthase (eNOS) Activity, and eNOS Coupling in Vivo

## Insights From Transgenic Mice With Endothelial-Targeted GTP Cyclohydrolase 1 and eNOS Overexpression

Jennifer K. Bendall, Nicholas J. Alp, Nicholas Warrick, Shijie Cai, David Adlam, Kirk Rockett, Mitsuhiro Yokoyama, Seinosuke Kawashima, Keith M. Channon

**Abstract**—Endothelial dysfunction in vascular disease states is associated with reduced NO bioactivity and increased superoxide ( $O_2^{\cdot-}$ ) production. Some data suggest that an important mechanism underlying endothelial dysfunction is endothelial NO synthase (eNOS) uncoupling, whereby eNOS generates  $O_2^{\cdot-}$  rather than NO, possibly because of a mismatch between eNOS protein and its cofactor tetrahydrobiopterin (BH4). However, the mechanistic relationship between BH4 availability and eNOS coupling in vivo remains undefined because no studies have investigated the regulation of eNOS by BH4 in the absence of vascular disease states that cause pathological oxidative stress through multiple mechanisms. We investigated the stoichiometry of BH4–eNOS interactions in vivo by crossing endothelial-targeted eNOS transgenic (eNOS-Tg) mice with mice overexpressing endothelial GTP cyclohydrolase 1 (GCH-Tg), the rate-limiting enzyme in BH4 synthesis. eNOS protein was increased 8-fold in eNOS-Tg and eNOS/GCH-Tg mice compared with wild type. The ratio of eNOS dimer:monomer was significantly reduced in aortas from eNOS-Tg mice compared with wild-type mice but restored to normal in eNOS/GCH-Tg mice. NO synthesis was elevated by 2-fold in GCH-Tg and eNOS-Tg mice but by 4-fold in eNOS/GCH-Tg mice compared with wild type. Aortic BH4 levels were elevated in GCH-Tg and maintained in eNOS/GCH-Tg mice but depleted in eNOS-Tg mice compared with wild type. Aortic and cardiac  $O_2^{\cdot-}$  production was significantly increased in eNOS-Tg mice compared with wild type but was normalized after NOS inhibition with *N* $\omega$ -nitro-L-arginine methyl ester hydrochloride (L-NAME), suggesting  $O_2^{\cdot-}$  production by uncoupled eNOS. In contrast, in eNOS/GCH-Tg mice,  $O_2^{\cdot-}$  production was similar to wild type, and L-NAME had no effect, indicating preserved eNOS coupling. These data indicate that eNOS coupling is directly related to eNOS–BH4 stoichiometry even in the absence of a vascular disease state. Endothelial BH4 availability is a pivotal regulator of eNOS activity and enzymatic coupling in vivo. (*Circ Res.* 2005;97:864-871.)

**Key Words:** endothelial nitric oxide synthase ■ tetrahydrobiopterin ■ nitric oxide ■ superoxide

Nitric oxide (NO), produced by endothelial NO synthase (eNOS) in the vascular endothelium, is a critical signaling molecule in vascular homeostasis.<sup>1</sup> NO serves as an endothelium-derived relaxing factor, regulates vasomotor tone and blood pressure,<sup>1,2</sup> and has multiple antiatherogenic roles by inhibiting vascular smooth muscle cell proliferation, platelet aggregation, and leukocyte adhesion.<sup>1</sup> Loss of NO bioavailability is a key feature of endothelial dysfunction in vascular disease states such as hypertension, diabetes, and atherosclerosis. Furthermore, impaired NO-mediated endothelial function is an independent risk factor for cardiovascular disease.<sup>3–5</sup> Several factors contribute to loss of NO

bioavailability, including reduced NO synthesis and NO scavenging by reactive oxygen species (ROS).<sup>6</sup> Under physiological conditions, there is a balance between endothelial NO and ROS production. However, vascular diseases are associated with increased ROS generation.<sup>6</sup> Several oxidase systems contribute to the increased oxidative stress, notably the NADPH oxidases.<sup>7,8</sup>

Increasing evidence suggests that eNOS itself can generate superoxide ( $O_2^{\cdot-}$ ) under certain pathophysiological conditions.<sup>9</sup> Ozaki et al<sup>10</sup> reported recently that transgenic overexpression of eNOS in apolipoprotein E knockout mice paradoxically increases vascular  $O_2^{\cdot-}$  production because of

Original received March 9, 2005; revision received August 10, 2004; accepted September 12, 2005.

From the Department of Cardiovascular Medicine (J.K.B., N.J.A., N.W., S.C., D.A., K.M.C.), University of Oxford, John Radcliffe Hospital, United Kingdom; Childhood Infection Group (K.R.), Wellcome Trust Centre for Human Genetics, University of Oxford, United Kingdom; and Kobe University School of Medicine (M.Y., S.K.), Japan.

Correspondence to Professor Keith M. Channon, Department of Cardiovascular Medicine, John Radcliffe Hospital, Oxford, OX3 9DU, UK. E-mail keith.channon@cardiov.ox.ac.uk

© 2005 American Heart Association, Inc.

*Circulation Research* is available at <http://circres.ahajournals.org>

DOI: 10.1161/01.RES.0000187447.03525.72

enzymatic uncoupling of increased eNOS protein levels. Recent data indicate that the pterin cofactor tetrahydrobiopterin (BH4) is a major determinant of whether eNOS produces NO or  $O_2^{\cdot-}$ .<sup>11,12</sup> When BH4 levels are insufficient, there is a shift toward the production of  $O_2^{\cdot-}$  as electron transfer within the active site of eNOS becomes uncoupled from L-arginine oxidation, and molecular oxygen is instead reduced to form  $O_2^{\cdot-}$ .<sup>11</sup>  $O_2^{\cdot-}$  generated by eNOS has been implicated in endothelial dysfunction associated with a number of vascular disease states, including diabetes, smoking, hypertension, and atherosclerosis,<sup>10,12–16</sup> and BH4 supplementation improves endothelium-dependent vasodilatation under these conditions.<sup>16</sup> However, the effects of systemic pharmacological BH4 supplementation in these studies may be mediated in part by nonspecific antioxidant properties of acute high-dose BH4,<sup>17</sup> which can increase NO bioavailability indirectly by reducing its scavenging by ROS.

Recent studies have focused on the potential role of BH4 oxidation, to dihydrobiopterin (BH2) and other biopterin species, in reducing BH4 bioavailability in preatherosclerotic disease states.<sup>16–18</sup> In particular, the interaction of BH4 with peroxynitrite (generated from the reaction between NO and  $O_2^{\cdot-}$ ) rapidly oxidizes BH4 and can provoke eNOS uncoupling and endothelial dysfunction.<sup>12,19–21</sup> Indeed, eNOS uncoupling may exacerbate the process by contributing to BH4 oxidation. However, it is unclear whether eNOS uncoupling alone is sufficient to initiate BH4 oxidation and exacerbate eNOS uncoupling *in vivo* because all *in vivo* studies to date have evaluated BH4-dependent eNOS regulation in complex vascular disease states in which multiple inflammatory and redox pathways are implicated. Other previous studies of the role of BH4 in eNOS function have relied on purified recombinant proteins in reconstituted cell-free systems.<sup>9,11,22,23</sup>

Accordingly, we sought to investigate the importance of BH4 in regulating eNOS activity *in vivo* in healthy animals without vascular disease. We used a transgenic mouse model with endothelial-targeted overexpression of GTP cyclohydrolase 1 (GTPCH), the rate-limiting enzyme in BH4 synthesis, in which endothelial BH4 levels are specifically increased.<sup>24</sup> We crossed this transgenic mouse with a mouse overexpressing eNOS in the endothelium to generate mouse models with graded alterations in endothelial BH4 and eNOS levels to investigate the mechanistic relationships between BH4 and eNOS coupling *in vivo*.

## Materials and Methods

### Animals

All studies involving laboratory animals were conducted in accordance with the UK Home Office Animals (Scientific Procedures) Act 1986 (HMSO, UK). eNOS transgenic (eNOS-Tg) mice, in which bovine eNOS transgene overexpression is targeted to the vascular endothelium under the control of the murine preproendothelin-1 promoter in a C57BL/6 background, were produced as described previously.<sup>25</sup> GTPCH transgenic (GCH-Tg) mice, in which human GTPCH transgene overexpression is targeted to the endothelium under control of the murine Tie-2 promoter, were generated in a C57BL/6 background as described previously.<sup>26</sup> Heterozygote eNOS-Tg mice were mated with heterozygote GCH-Tg mice to produce experimental eNOS/GCH-Tg, eNOS-Tg, GCH-Tg, and wild-type littermates in a 1:1:1:1 ratio. Mice (between 13 and 20

weeks of age in all experiments) were housed in individually ventilated cages with 12-hour light/dark cycle and controlled temperature (20°C to 22°C) and fed normal chow and water *ad libitum*.

### Western Blot Analysis

Lung samples ( $n \geq 4$  per group) were homogenized on ice for 20 seconds in lysis buffer (50 mmol/L Tris, pH 7.5, 150 mmol/L NaCl, 0.1% SDS, 0.5% deoxycholate, 1% Nonidet P-40) containing protease inhibitors (Complete; Boehringer Mannheim) and 1 mmol/L phenylmethylsulfonyl fluoride. Protein lysates (8  $\mu$ g) were resolved using SDS-PAGE and transferred to polyvinylidene difluoride membranes. Membranes were incubated with a 1:2000 dilution of mouse anti-eNOS monoclonal antibody (Transduction Laboratories), which recognizes murine and bovine eNOS, followed by a 1:2500 dilution of rabbit anti-mouse horseradish peroxidase-conjugated secondary antibody (Promega). Protein bands were visualized by chemiluminescence. To investigate the ratio of eNOS homodimer to monomer, Western blots were performed as above using nonboiled aortic lysates and low-temperature SDS-PAGE as described previously.<sup>27</sup>

### Primary Cultures of Murine Lung Endothelial Cells

Lungs were harvested into culture medium (35% DMEM, 35% Ham's F-10 nutrient mixture, 20% FBS, 2 mmol/L L-glutamine, 100 U/100  $\mu$ g/mL penicillin-streptomycin, 100  $\mu$ g/mL heparin, and 50  $\mu$ g/mL endothelial mitogen [Biogenesis]), cut into 1- to 2-mm pieces and digested using 0.1% collagenase type 1 for 1 hour at 37°C. The lung digest was passed through a 100- $\mu$ m cell strainer. Cells were centrifuged, resuspended in culture medium, and plated onto 0.1% gelatin-coated cover slips. Cultures were maintained at 37°C in humidified 5% CO<sub>2</sub>/95% air atmosphere for 72 hours before fixation with 4% paraformaldehyde.

### Immunocytochemistry

Fixed cultures were permeabilized with PBS containing 0.5% Triton X-100, and nonspecific staining was reduced by blocking with 10% normal goat serum. Cultures were incubated with a polyclonal rabbit anti-eNOS primary antibody (Transduction Laboratories) followed by goat anti-rabbit secondary antibody (Alexa Fluor 488; Molecular Probes). Cells were mounted with cover slips using Vectashield containing propidium iodide (Vector Laboratories) and imaged using a Bio-Rad MRC-1024 laser-scanning confocal microscope.

### Measurement of Biopterins and Neopterin

Biopterins, such as BH4, BH2 and biopterin, and neopterin were measured in aortic homogenates by high-performance liquid chromatography (HPLC) analysis after iodine oxidation in acidic or alkaline conditions as described previously.<sup>24,28</sup> In brief, thoracic aortas ( $n=6$  to 8 per group) were homogenized for 20 seconds in ice-cold extract buffer (50 mmol/L Tris-HCl, pH 7.4, 1 mmol/L dithiothreitol, and 1 mmol/L EDTA) containing 0.1  $\mu$ mol/L neopterin as an internal recovery standard. Samples were deproteinized before undergoing oxidation with 1% iodine/2% potassium iodide under either acidic or basic conditions. Biopterin content was assessed using HPLC in 5% methanol/95% water using an ACE 5 C18 column (ACT) and fluorescence detection (350 nm excitation and 450 nm emission). BH4 concentration was calculated as picomoles per milligram of protein by subtracting BH2 and biopterin from total biopterin content.

### Arginine-to-Citrulline Conversion

NOS enzymatic activity, and indirectly NO synthesis, was measured by the conversion of <sup>14</sup>C L-arginine to <sup>14</sup>C L-citrulline in fresh intact aorta ( $n=5$  to 8 per group) and lung homogenate ( $n=6$  per group) as described previously.<sup>24,29</sup> The integrals of citrulline peaks were expressed as a proportion of total <sup>14</sup>C counts for each sample.

### Electron Paramagnetic Resonance Spectroscopy

Electron paramagnetic resonance (EPR) spectroscopy was used to quantify vascular NO production according to previously described and validated methods.<sup>30</sup> In brief, freshly harvested aortas (n=8 to 11 per group) were stimulated with calcium ionophore (A23187; 1  $\mu\text{mol/L}$ ) in 100  $\mu\text{L}$  Krebs-HEPES buffer, then incubated with colloid iron (II) diethyldithiocarbamate [ $\text{Fe}(\text{DETC})_2$ ] (285  $\mu\text{mol/L}$ ) at 37°C for 90 minutes. After incubation, aortas were snap-frozen in a column of Krebs-HEPES buffer in liquid nitrogen, and EPR spectra were obtained using an X-band EPR spectrometer (Miniscope MS 200; Magnetech). Signals were quantified by measuring the total amplitude, after correction of baseline, and after subtracting background signals from incubation with colloid  $\text{Fe}(\text{DETC})_2$  alone.

### Lucigenin-Enhanced Chemiluminescence Detection of Superoxide in Heart Lysates

Basal  $\text{O}_2^{\cdot -}$  production was measured in left ventricular (LV) homogenates (n=7 to 10 per group) using the technique of lucigenin (5  $\mu\text{mol/L}$ ) chemiluminescence according to methods described previously.<sup>14,31</sup> In brief, hearts were flushed with ice-cold Krebs-HEPES buffer, the LV excised, and snap-frozen in liquid nitrogen. Samples were homogenized in Krebs-HEPES buffer containing protease inhibitors (Complete; Boehringer Mannheim) at pH 7.4. Chemiluminescence was measured in a FB12 luminometer (Berthold Detection Systems) at 37°C. Chemiluminescence of 200  $\mu\text{g}$  LV protein was recorded every minute for 8 minutes. The NOS inhibitor *N* $\omega$ -nitro-L-arginine methyl ester hydrochloride (L-NAME; 1 mmol/L) was subsequently added and chemiluminescence recorded for an additional 5 minutes. Background readings were subtracted from sample readings and results expressed as counts per second.

### Lucigenin-Enhanced Chemiluminescence Detection of Superoxide in Intact Aorta

Basal  $\text{O}_2^{\cdot -}$  production was measured in intact aorta (n=8 to 12 per group) according to methods described previously.<sup>14,32</sup> In brief, freshly cleaned and harvested thoracic aortas were opened longitudinally, cut into 2, and transferred to ice-cold Krebs-HEPES buffer. Vessels were equilibrated in Krebs-HEPES buffer gassed with 95% oxygen/5% carbon dioxide for 30 minutes at 37°C, with one half of each vessel being incubated in the presence of L-NAME (1 mmol/L). Lucigenin (20  $\mu\text{mol/L}$ ) chemiluminescence was then recorded every minute for 10 minutes as above. Background readings were subtracted from sample readings and results expressed as counts per second per milligram dry weight of aorta.

### Oxidative Fluorescent Microtopography

$\text{O}_2^{\cdot -}$  production in tissue sections of mouse aorta (n=5 to 7 per group) was detected using the fluorescent probe dihydroethidium (DHE), as described previously.<sup>14,24,33</sup> Fresh segments of thoracic aorta were frozen in optimal cutting temperature compound. Cryosections (30  $\mu\text{m}$ ) were incubated with Krebs-HEPES buffer with or without L-NAME (1 mmol/L; to inhibit eNOS) for 30 minutes at 37°C, then for an additional 5 minutes with DHE (2  $\mu\text{mol/L}$ ; Molecular Probes). Images were obtained using a Bio-Rad laser-scanning confocal microscope, equipped with a krypton/argon laser, using identical acquisition settings for each section. DHE fluorescence was quantified by automated image analysis using Image-Pro Plus software (Media Cybernetics). DHE fluorescence from high power ( $\times 60$ ) images was measured only on the luminal side of the internal elastic lamina to quantify endothelial cell fluorescence. For each vessel, mean fluorescence was calculated from 4 separate high-power fields taken in each quadrant of the vessel to produce n=1, and all experiments were performed in a batch design.

### Statistical Analysis

One-way ANOVA tests were used to compare data sets, with appropriate post hoc correction for multiple comparisons.  $P < 0.05$  was considered significant. Data are expressed as means and SEM.

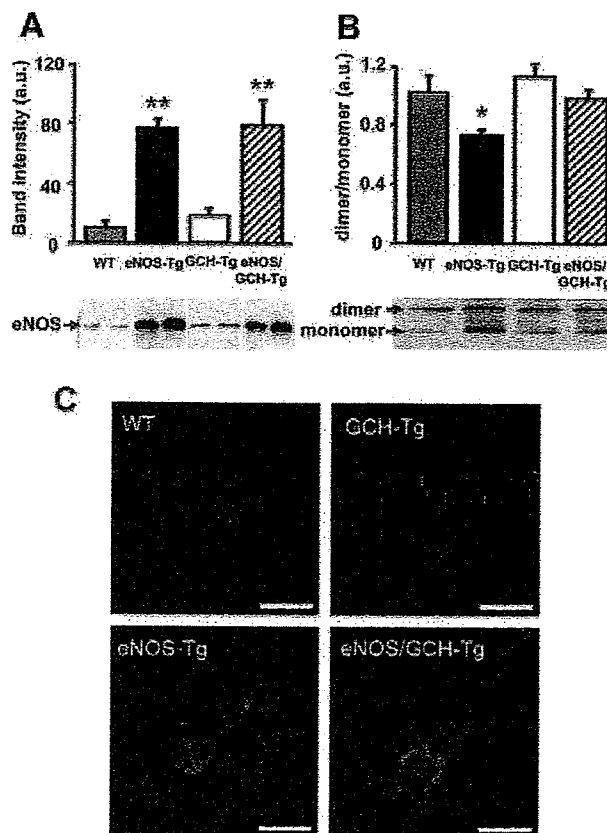


**Figure 1.** Immunoblotting with a murine anti-eNOS monoclonal antibody to detect native and transgenic eNOS monomer protein in boiled lung lysates (A) and eNOS dimer:monomer protein bands in aortic lysates from wild-type (WT), eNOS-Tg, GCH-Tg, and eNOS/GCH-Tg mice (B); n=4 animals per group; \* $P < 0.05$  and \*\* $P < 0.001$  compared with WT. a.u. indicates arbitrary units. C, Immunofluorescent detection of eNOS (green), counterstained with propidium iodide (red), in primary endothelial cells cultured from WT, eNOS-Tg, GCH-Tg, and eNOS/GCH-Tg mice. Bar=20  $\mu\text{m}$ .

## Results

### eNOS Protein Levels and Subcellular Localization

Western blot analysis confirmed that eNOS protein levels were elevated 8-fold in eNOS-Tg compared with wild-type animals ( $P < 0.001$ ; Figure 1A). Overexpression of endothelial GTPCH, the rate-limiting enzyme in BH4 synthesis, in GCH-Tg mice did not significantly alter eNOS protein levels compared with wild type. However, as for eNOS-Tg mice, eNOS protein levels were elevated 8-fold in double-transgenic eNOS/GCH-Tg mice.

We used low-temperature SDS-PAGE and immunoblotting to investigate eNOS homodimerization and the ratio of eNOS dimer to monomer in aortas. In eNOS-Tg aortas, eNOS dimer:monomer was significantly depleted compared with wild type ( $P < 0.05$ ) but unchanged in GCH-Tg mice (Figure 1B). Importantly, the reduced eNOS dimer:monomer ratio in the eNOS-Tg group was restored to wild-type levels in double-transgenic eNOS/GCH-Tg mice.

We investigated the subcellular localization of eNOS in primary cultures of lung endothelial cells using immunocytochemistry. eNOS appeared to be localized mainly to plasma

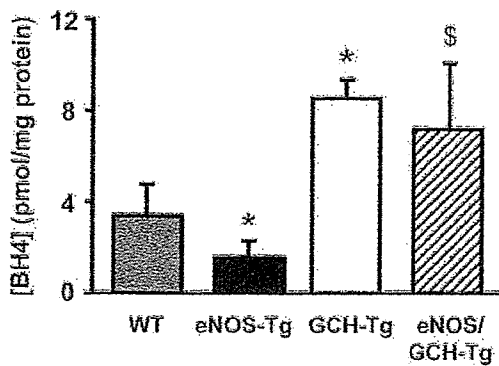


Figure 2. BH4 levels in aortas from wild-type (WT), eNOS-Tg, GCH-Tg, and eNOS/GCH-Tg mice. \**P*<0.05 compared with WT and \$*P*<0.05 compared with eNOS-Tg; n=6 to 8 animals per group.

membranes and the Golgi apparatus in endothelial cells from all 4 groups (Figure 1C). However, in accordance with the immunoblotting data, the intensity of eNOS immunostaining, unchanged in GCH-Tg mice, was markedly increased in endothelial cells from eNOS-Tg and eNOS/GCH-Tg animals compared with wild type.

**Aortic BH4 Levels**

We next measured vascular BH4 levels in homogenates of snap-frozen aorta using iodine oxidation and HPLC. Surprisingly, BH4 levels were significantly depleted in eNOS-Tg mice compared with wild type, suggesting oxidative degradation of BH4 (*P*<0.05; Figure 2). We then sought to confirm that increased endothelial GTPCH expression led to increased BH4 levels in aortic homogenates of GCH-Tg and eNOS/GCH-Tg mice. As reported previously,<sup>24</sup> aortic BH4 levels were significantly elevated by >2-fold in GCH-Tg mice compared with wild type (*P*<0.05). Importantly, aortic BH4 levels were also elevated in eNOS/GCH-Tg mice and were not significantly different between GCH-Tg and eNOS/GCH-Tg mice.

**eNOS Enzymatic Activity and NO Production**

To determine the relationship between eNOS protein levels and eNOS enzymatic activity, we measured conversion of <sup>14</sup>C L-arginine to <sup>14</sup>C L-citrulline by eNOS in intact aorta using HPLC with online scintillation detection. Citrulline production was increased only 2-fold in eNOS-Tg aortas compared with wild type (*P*<0.05; Figure 3A and 3B), despite eNOS protein levels being elevated 8-fold in these animals. Indeed, the ratio of eNOS enzymatic activity to eNOS protein was 0.6 in eNOS-Tg mice compared with 2.0 in wild-type animals. A similar pattern of results was obtained when using lung tissue lysates (Figure 3C). To further investigate the stoichiometric relationship between eNOS and endothelial BH4 in vivo and to determine whether increasing endothelial BH4 in eNOS-Tg mice could augment eNOS enzymatic activity, we next measured eNOS enzymatic activity in GCH-Tg and eNOS/GCH-Tg mice. NOS activity was increased 2-fold in GCH-Tg aorta and lung compared with wild type (*P*<0.05; Figure 3A through 3C). Indeed, eNOS enzymatic activity was similar in GCH-Tg and eNOS-Tg mice despite eNOS protein

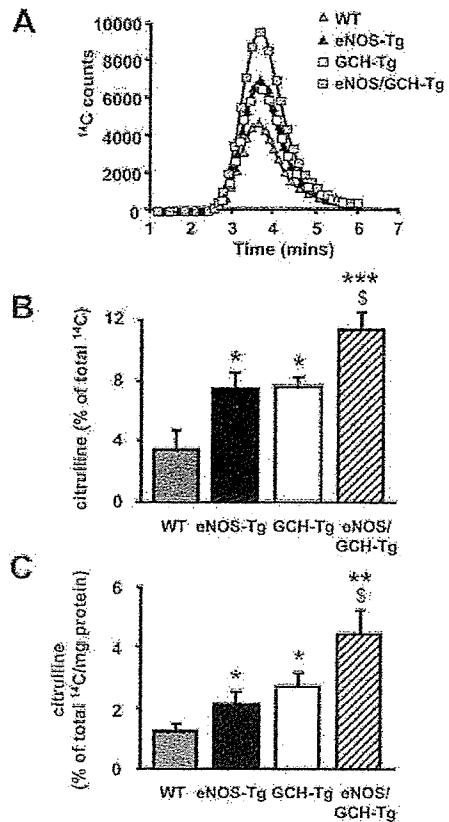
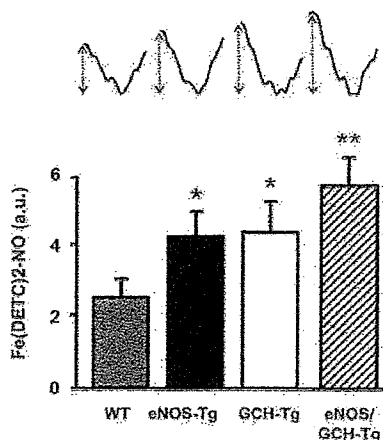


Figure 3. A, Representative HPLC chromatograms showing <sup>14</sup>C citrulline peaks for wild-type (WT; gray triangles), eNOS-Tg (black triangles), GCH-Tg (white squares), and eNOS/GCH-Tg (hatched squares) mouse aortas. Graphs show percentage <sup>14</sup>C citrulline conversion from <sup>14</sup>C arginine as a measure of eNOS activity measured in total fresh intact aorta (B) and lung tissue lysates (C); n=5 to 8 animals per group; \**P*<0.05, \*\**P*<0.01, and \*\*\**P*<0.001 compared with WT; and \$*P*<0.05 compared with eNOS-Tg.

levels being considerably higher in eNOS-Tg animals. Critically, eNOS enzymatic activity was further elevated in eNOS/GCH-Tg mice compared with eNOS-Tg animals (*P*<0.05): augmented levels of endothelial BH4 in eNOS/GCH-Tg mice resulted in an ≈4-fold increase in eNOS enzymatic activity in aorta and lung compared with wild-type mice (*P*<0.01). These data suggest that eNOS activity is exquisitely dependent on endothelial BH4 levels even in the absence of vascular disease.

In complementary experiments, we used Fe-DETC EPR to directly measure NO bioavailability in mouse aortas. In accordance with measures of enzymatic activity, net NO levels were increased ≈2-fold in eNOS-Tg aortas compared with wild type (Figure 4). These results demonstrate that there was a striking discordance between eNOS protein levels, eNOS enzymatic activity, and NO production in eNOS-Tg mice. We then determined the effects of increased endothelial BH4 using the GCH-Tg and eNOS/GCH-Tg mice and observed a similar pattern of results as for NOS enzymatic activity. Aortic NO bioavailability was elevated almost 2-fold in GCH-Tg mice compared with wild type and not significantly different from eNOS-Tg mice (Figure 4). Criti-



**Figure 4.** Net NO levels in intact aorta measured using Fe-DETC EPR. Graph shows mean quantitative data with corresponding representative EPR spectra showing the characteristic peaks associated with the Fe-DETC signal above.  $n=8$  to 11 animals per group; \* $P<0.05$  and \*\* $P<0.01$  compared with wild type (WT). a.u. indicates arbitrary units.

cally, net NO bioavailability was further elevated ( $\approx 3$ -fold compared with wild type) in eNOS/GCH-Tg mice.

#### eNOS Uncoupling: Effect of eNOS and GTPCH Overexpression In Vivo

To investigate whether eNOS uncoupling results from discordance between eNOS and BH4, we measured  $O_2^{\cdot -}$  production and, more specifically, eNOS-derived  $O_2^{\cdot -}$  production using the NOS inhibitor L-NAME. We first measured  $O_2^{\cdot -}$  production in tissue lysates using lucigenin chemiluminescence. Chemiluminescence was increased 2-fold in eNOS-Tg mice compared with wild-type animals ( $P<0.05$ ; Figure 5A) but was unchanged in GCH-Tg mice. Critically,  $O_2^{\cdot -}$  production was restored in eNOS/GCH-Tg mice. The proportion of  $O_2^{\cdot -}$  production attributable to uncoupled NOS, assessed by quantifying L-NAME-inhibitable chemiluminescence, was significantly increased in eNOS-Tg lysates compared with wild type, indicating increased NOS uncoupling ( $P<0.05$ ; Figure 5B). L-NAME-inhibitable chemilumines-

#### Lucigenin Chemiluminescence to Measure $O_2^{\cdot -}$ Production in Intact Aortas Incubated for 30 Minutes at 37°C in the Presence or Absence of L-NAME (1 mmol/L)

	Wild Type	eNOS-Tg	GCH-Tg	eNOS/GCH-Tg
Basal, RLU/s/mg	39.5 $\pm$ 4.5	59.7 $\pm$ 6.6*	52.8 $\pm$ 5.8	46.2 $\pm$ 4.7
+ L-NAME, RLU/s/mg	42.5 $\pm$ 10.1	39.2 $\pm$ 4.8†	54.0 $\pm$ 13.2	49.3 $\pm$ 11.2

Results are expressed as counts per second per milligram of dry weight of aorta.

\* $P<0.05$  compared with wild type; † $P<0.05$  compared with baseline (without L-NAME).

RLU indicates relative light units.

cence was unchanged in GCH-Tg mice. The presence of the GTPCH transgene in eNOS/GCH-Tg mice restored the enhanced L-NAME-inhibitable chemiluminescence of the eNOS-Tg group back to wild-type levels. We also investigated  $O_2^{\cdot -}$  production in intact aorta under basal conditions and after incubation with L-NAME using lucigenin chemiluminescence and saw a similar pattern of results. Basal chemiluminescence was significantly increased in eNOS-Tg aortas compared with wild type ( $P<0.05$ ; Table). Importantly, basal  $O_2^{\cdot -}$  production in GCH-Tg and eNOS/GCH-Tg aortas was similar to wild type. Incubation of aortas with L-NAME caused a significant reduction in the  $O_2^{\cdot -}$  signal in eNOS-Tg mice ( $P<0.05$ ), indicating NOS uncoupling. However, L-NAME had little effect in wild-type, GCH-Tg, and eNOS/GCH-Tg aortas, suggesting that NOS coupling is preserved in these mice. Together, these observations suggest that in eNOS-Tg mice elevated  $O_2^{\cdot -}$  production is at least partly attributable to uncoupled NOS, likely resulting from discordance between eNOS protein and endothelial BH4 because NOS coupling is preserved by increasing endothelial BH4 in association with elevated eNOS levels in eNOS/GCH-Tg animals.

To investigate  $O_2^{\cdot -}$  production specifically from the aortic endothelium, we quantified endothelial DHE fluorescence using oxidative confocal microtopography. Endothelial DHE fluorescence was increased 2-fold in eNOS-Tg mice compared with wild-type and GCH-Tg mice (Figure 6). Impor-

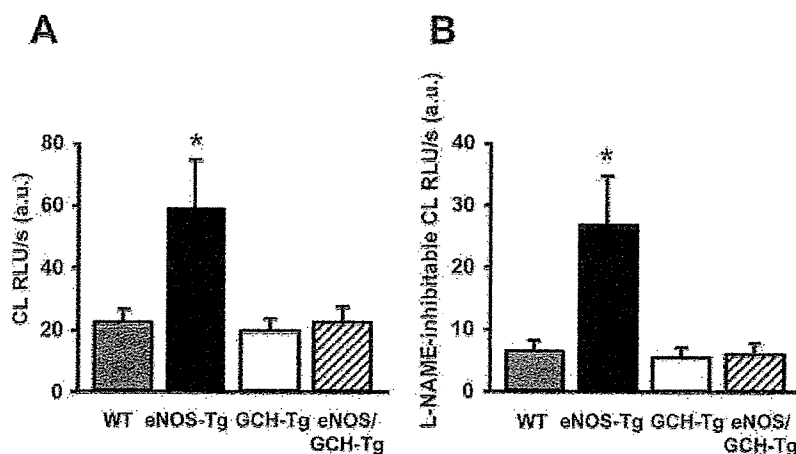


**Figure 5.** Lucigenin (5  $\mu$ mol/L) chemiluminescence (CL) in cardiac tissue lysates from wild-type (WT), eNOS-Tg, GCH-Tg, and eNOS/GCH-Tg mice to measure basal  $O_2^{\cdot -}$  production (A) and L-NAME (1 mmol/L)-inhibitable  $O_2^{\cdot -}$  production (B) as a marker of NOS uncoupling. \* $P<0.05$  compared with WT;  $n=7$  to 10 animals per group. RLU indicates relative light units; a.u., arbitrary units.

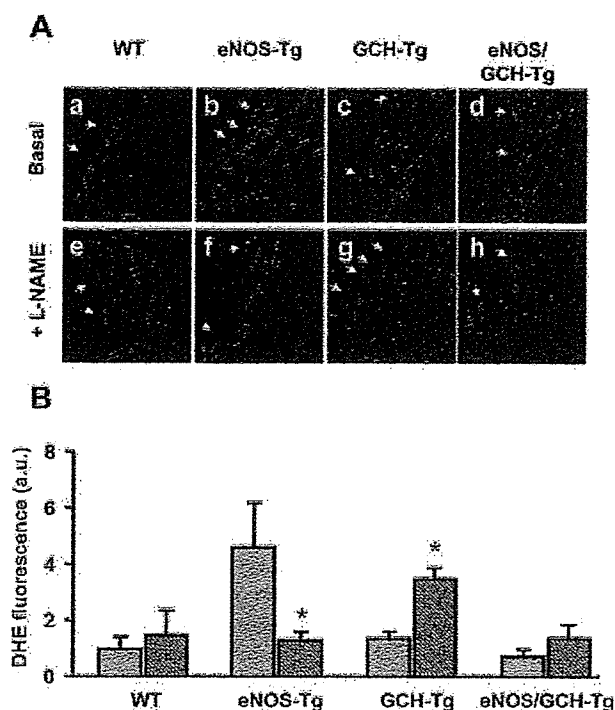


**Figure 6.** DHE staining, to measure in situ  $O_2^{\cdot-}$  production, in aortic sections. **A**, Representative aortic sections ( $\times 60$ ) showing red endothelial cells (arrows) from wild-type (WT; **a** and **e**), eNOS-Tg (**b** and **f**), GCH-Tg (**c** and **g**), and eNOS/GCH-Tg (**d** and **h**) mice in the presence (**e** through **h**) and absence (**a** through **d**) of L-NAME (1 mmol/L). **B**, Quantified specific endothelial DHE fluorescence is expressed for sections in the presence (hatched bars) and absence (gray bars) of L-NAME in arbitrary units (a.u.) for each group. \* $P < 0.05$  comparing sections in the presence or absence of L-NAME;  $n = 5$  to 7 animals per group.

tantly, endothelial fluorescence was restored to wild-type levels in eNOS/GCH-Tg mice. Fluorescence from the other layers of the vessel wall was not significantly different between groups. Incubation with L-NAME had little effect in wild-type aortas but reversed the elevated DHE signal in eNOS-Tg endothelium back to wild-type levels, again indicating that the source of  $O_2^{\cdot-}$  was likely uncoupled eNOS. In contrast, L-NAME significantly increased the endothelial  $O_2^{\cdot-}$  signal in GCH-Tg mice, indicating that in these aortas, eNOS was predominantly coupled and producing NO. Critically, as in wild-type aortas, NOS inhibition with L-NAME had little effect in eNOS/GCH-Tg mice, indicating restored eNOS coupling compared with eNOS-Tg animals. In accordance with the data for  $O_2^{\cdot-}$  production measured by chemiluminescence, these results suggest that increased eNOS uncoupling in eNOS-Tg aortas increases eNOS-derived  $O_2^{\cdot-}$ , but that eNOS coupling is, at least in part, preserved by increased endothelial BH4 synthesis in eNOS/GCH-Tg mice.

### Discussion

In this study, we describe a new double-transgenic mouse model in which endothelial-targeted overexpression of GTPCH leads to increased endothelial BH4 levels in mice with endothelial-targeted eNOS overexpression. We used this model to investigate the role of BH4 in the regulation of

eNOS coupling in vivo, specifically in the absence of pathological oxidative stress associated with vascular disease states.<sup>6</sup> The major findings in this study are as follows. First, eNOS protein levels are markedly elevated in eNOS-Tg and eNOS/GCH-Tg mice but not in GCH-Tg animals, although the proportion of eNOS dimer to monomer is depleted only in eNOS-Tg aortas. Second, endothelial-specific overexpression of GTPCH is sufficient to increase vascular BH4 levels in GCH-Tg and in eNOS/GCH-Tg aortas, whereas BH4 levels are depleted in eNOS-Tg aortas. Third, this increase in BH4 is sufficient to augment vascular eNOS enzymatic activity even in GCH-Tg mice, which have unchanged eNOS protein levels. Indeed, eNOS activity is similar between GCH-Tg and eNOS-Tg mice despite eNOS-Tg mice having 8-fold more eNOS protein. Importantly, the increase in endothelial BH4 in eNOS/GCH-Tg mice further enhances eNOS activity and NO bioavailability compared with eNOS-Tg mice. Fourth, the discordance between endothelial BH4 and eNOS protein in eNOS-Tg mice results in uncoupled eNOS and increased NOS-derived  $O_2^{\cdot-}$  production in tissue lysates and intact aorta. However, increased vascular BH4 in eNOS/GCH-Tg mice is sufficient, at least in part, to restore eNOS coupling, increase NO production, and reduce eNOS-dependent  $O_2^{\cdot-}$  production.

These findings provide important insights into the role of endothelial BH4 synthesis in regulating eNOS activity and eNOS coupling even in the absence of vascular oxidative stress. Previous studies have reported that endothelial dysfunction in vascular diseases, such as hypertension,<sup>12</sup> diabetes,<sup>24</sup> and atherosclerosis,<sup>26</sup> is associated with increased  $O_2^{\cdot-}$  production deriving principally from NADPH oxidases.<sup>7,8</sup> Landmesser et al<sup>12</sup> demonstrated that the increase in NADPH oxidase-derived  $O_2^{\cdot-}$  in deoxycorticosterone acetate-salt hypertensive mice led to enhanced oxidation of BH4, resulting in eNOS uncoupling, increased eNOS-derived  $O_2^{\cdot-}$  production, and reduced NO formation, thereby exacerbating oxidative stress. Oral supplementation with BH4, or a reduction in NADPH oxidase activity (using p47phox<sup>-/-</sup> mice), reversed eNOS uncoupling. However, the mechanistic relationship between eNOS and its cofactor BH4 has not been investigated in vivo in the absence of pathological oxidative stress. We now show that a stoichiometric discordance between eNOS protein and BH4 levels is alone sufficient to cause eNOS uncoupling, and that eNOS uncoupling in the absence of vascular disease is sufficient to deplete BH4 levels by oxidation. Laursen et al<sup>19</sup> demonstrated that peroxynitrite may be the principal ROS involved in oxidation of BH4.

NO, constitutively produced by eNOS in the vascular endothelium, is a potent vasodilator and exerts numerous vasoprotective antiatherogenic effects. Reduced NO bioactivity is an early feature of a number of vascular diseases, including atherosclerosis.<sup>5</sup> Short-term in vivo gene transfer of eNOS or neuronal NOS can improve NO-mediated vascular relaxation in atherosclerotic arteries.<sup>34</sup> However, previous studies investigating the possible vasoprotective effects of chronic eNOS overexpression in eNOS-Tg mice have yielded conflicting results. Kawashima et al<sup>35</sup> demonstrated reduced lesion formation after carotid artery ligation in eNOS-Tg mice. In contrast, Ozaki et al,<sup>10</sup> using the same strain of



eNOS-Tg mice as used in the present study, found that eNOS overexpression accelerated rather than reduced atherosclerosis in apolipoprotein E knockout mice, at least in part, because of eNOS uncoupling and  $O_2^{\cdot-}$  generation. In the present study, using a mouse model not exposed to pathological vascular oxidative stress, we also show that eNOS-derived  $O_2^{\cdot-}$  production is enhanced in eNOS-Tg mice, in cardiac tissue lysates and intact aorta, indicating increased eNOS uncoupling in these animals. We performed additional experiments, using quantitative RT-PCR, to confirm that the increased  $O_2^{\cdot-}$  in eNOS-Tg animals is not a result of a concomitant increase in the expression of the NADPH oxidase system, a major source of vascular  $O_2^{\cdot-}$  generation (data not shown). These findings agree with those from Ohashi et al<sup>25</sup> using nondiseased eNOS-Tg mice. This enhanced vascular oxidative stress may account for the depleted aortic BH4 levels observed in the eNOS-Tg mice because BH4 is readily oxidized by ROS to BH2 that is inactive for eNOS cofactor function. In accordance with having increased uncoupled eNOS and depleted BH4 levels, specific NOS enzymatic activity is markedly attenuated in eNOS-Tg mice (elevated only 2-fold compared with wild type) relative to eNOS protein levels (elevated 8-fold compared with wild type). Indeed, the ratio of eNOS enzymatic activity to eNOS protein was only 0.6 in eNOS-Tg mice compared with 2.0 in wild-type animals.

Several previous studies have established that BH4 is a required cofactor for NOS activity.<sup>9,28,36</sup> Recent studies, including those in atherosclerotic eNOS-Tg mice,<sup>10</sup> have demonstrated that NOS uncoupling can be reversed and NOS enzymatic activity increased by augmenting BH4 levels.<sup>10,12</sup> However, an advantage of the present study is that by targeting overexpression of GTPCH, the rate-limiting enzyme in BH4 biosynthesis, to the vascular endothelium, we avoid the potential confounding antioxidant effects of high-dose pharmacological BH4 supplementation used in other studies.<sup>10,12</sup> Furthermore, we have been able to specifically evaluate the role of endothelial BH4, as opposed to systemic BH4, in the regulation of eNOS activity. Importantly, using 2 methods to measure  $O_2^{\cdot-}$  production in cardiac tissue and intact aorta, as well as specifically in aortic endothelium, we demonstrate that NOS-dependent  $O_2^{\cdot-}$  generation, elevated in eNOS-Tg mice, is normalized in eNOS/GCH-Tg mice. These data support the hypothesis that discordance between eNOS protein and endothelial BH4 levels is sufficient to cause eNOS uncoupling even in the absence of pathological oxidative stress. In support of this conclusion, NOS enzymatic activity and the ratio of enzymatic activity relative to eNOS protein levels were increased in eNOS/GCH-Tg compared with eNOS-Tg mice. Interestingly, GCH-Tg mice also had increased NOS enzymatic activity compared with wild type, indicating that even in the absence of either enhanced eNOS protein or disease, BH4 levels may limit eNOS enzymatic activity in vivo. These data therefore suggest that eNOS activity (to generate NO) can be augmented by modestly increasing BH4 levels, specifically in the endothelium, even under normal physiological conditions.

Previous data have shown that eNOS dimerization is an important aspect of eNOS activation and NO production.<sup>28</sup>

BH4 has been suggested to increase the stability of the eNOS homodimer such that the ratio of dimer to monomer is increased.<sup>28,37</sup> In eNOS-Tg mice, the discordance between high levels of eNOS protein and depleted aortic BH4 levels may account for the relative decrease in homodimeric eNOS protein that we observed. In support, the increased production of endothelial BH4 in eNOS/GCH-Tg mice was sufficient to maintain the ratio of eNOS dimer to monomer. These in vivo findings corroborate previous in vitro studies suggesting that an important action of BH4, in addition to its direct contribution to electron transport within the eNOS active site, is to maintain eNOS in its homodimeric conformation.

We conclude that eNOS uncoupling is an independent and direct consequence of a stoichiometric discordance between enzyme and its cofactor BH4. BH4 is critical for regulating eNOS activity and its production of NO, as opposed to  $O_2^{\cdot-}$ , even in the absence of increased oxidative stress associated with vascular disease states. Thus, strategies to increase eNOS protein without a concomitant augmentation of endothelial BH4 levels may lead to eNOS uncoupling and paradoxically exacerbate oxidative stress and the progression of vascular diseases. Although reduced biosynthesis of BH4 may not be the principal mechanism of BH4 loss in vascular disease, strategies aimed at increasing BH4 synthesis or reducing BH4 oxidation may be valid therapeutic approaches in vascular disease states.

### Acknowledgments

This work was supported by the British Heart Foundation (RG02/007) and the Wellcome Trust.


### References

- Ignarro LJ. Nitric oxide as a unique signaling molecule in the vascular system: a historical overview. *J Physiol Pharmacol*. 2002;53:503–514.
- Furchgott RF, Zawadzki JV. The obligatory role of endothelial cells in the relaxation of arterial smooth muscle by acetylcholine. *Nature*. 1980;288:373–376.
- Panza JA, Garcia CE, Kilcoyne CM, Quyyumi AA, Cannon RO III. Impaired endothelium-dependent vasodilation in patients with essential hypertension: evidence that nitric oxide abnormality is not localized to a single signal transduction pathway. *Circulation*. 1995;91:1732–1738.
- Schachinger V, Britten MB, Zeiler AM. Prognostic impact of coronary vasodilator dysfunction on adverse long-term outcome of coronary heart disease. *Circulation*. 2000;101:1899–1906.
- Heitzer T, Schlinzig T, Krohn K, Meinertz T, Munzel T. Endothelial dysfunction, oxidative stress, and risk of cardiovascular events in patients with coronary artery disease. *Circulation*. 2001;104:2673–2678.
- Cai H, Harrison DG. Endothelial dysfunction in cardiovascular diseases: the role of oxidant stress. *Circ Res*. 2000;87:840–844.
- Griendling KK, Sorrescu D, Ushio-Fukai M. NAD(P)H oxidase: role in cardiovascular biology and disease. *Circ Res*. 2000;86:494–501.
- Guzik TJ, West NEJ, Black E, McDonald D, Ratnatunga C, Pillai R, Channon KM. Vascular superoxide production by NAD(P)H oxidase: association with endothelial dysfunction and clinical risk factors. *Circ Res*. 2000;86:e85–e90.
- Vasquez-Vivar J, Kalyanaraman B, Martasek P, Hogg N, Masters BS, Karoui H, Tordo P, Pritchard KA Jr. Superoxide generation by endothelial nitric oxide synthase: the influence of cofactors. *Proc Natl Acad Sci U S A*. 1998;95:9220–9225.
- Ozaki M, Kawashima S, Yamashita T, Hirase T, Namiki M, Inoue N, Hirata K-i, Yasui H, Sakurai H, Yoshida Y, Masada M, Yokoyama M. Overexpression of endothelial nitric oxide synthase accelerates atherosclerotic lesion formation in apoE-deficient mice. *J Clin Invest*. 2002;110:331–340.
- Vasquez-Vivar J, Kalyanaraman B, Martasek P. The role of tetrahydrobiopterin in superoxide generation from eNOS: enzymology and physiological implications. *Free Radic Res*. 2003;37:121–127.

12. Landmesser U, Dikalov S, Price SR, McCann L, Fukui T, Holland SM, Mitch WE, Harrison DG. Oxidation of tetrahydrobiopterin leads to uncoupling of endothelial cell nitric oxide synthase in hypertension. *J Clin Invest.* 2003;111:1201–1209.
13. Maier W, Cosentino F, Lurati RB, Fleisch M, Seiler C, Hess OM, Meier B, Luscher TF. Tetrahydrobiopterin improves endothelial function in patients with coronary artery disease. *J Cardiovasc Pharmacol.* 2000;35:173–178.
14. Guzik TJ, Mussa S, Gastaldi D, Sadowski J, Ratanunga C, Pillai R, Channon KM. Mechanisms of increased vascular superoxide production in human diabetes mellitus: role of NAD(P)H oxidase and endothelial nitric oxide synthase. *Circulation.* 2002;105:1656–1662.
15. Heitzer T, Yla-Herttuala S, Luoma J, Kurz S, Munzel T, Just H, Olschewski M, Drexler H. Cigarette smoking potentiates endothelial dysfunction of forearm resistance vessels in patients with hypercholesterolemia. Role of oxidized LDL. *Circulation.* 1996;93:1346–1353.
16. Alp NJ, Channon KM. Regulation of endothelial nitric oxide synthase by tetrahydrobiopterin in vascular disease. *Arterioscler Thromb Vasc Biol.* 2004;24:413–420.
17. Vasquez-Vivar J, Whittsett J, Martasek P, Hogg N, Kalyanaraman B. Reaction of tetrahydrobiopterin with superoxide: EPR-kinetic analysis and characterization of the pteridine radical. *Free Radic Biol Med.* 2001;31:975–985.
18. Zheng J-S, Yang X-Q, Lookingland KJ, Fink GD, Hesslinger C, Kapatos G, Kovacs I, Chen AF. Gene transfer of human guanosine 5'-triphosphate cyclohydrolase I restores vascular tetrahydrobiopterin level and endothelial function in low renin hypertension. *Circulation.* 2003;108:1238–1245.
19. Laursen JB, Somers M, Kurz S, McCann L, Warnholtz A, Freeman BA, Tarpey M, Fukui T, Harrison DG. Endothelial regulation of vasomotion in apoE-deficient mice: implications for interactions between peroxynitrite and tetrahydrobiopterin. *Circulation.* 2001;103:1282–1288.
20. Kuzkaya N, Weissmann N, Harrison DG, Dikalov S. Interactions of peroxynitrite, tetrahydrobiopterin, ascorbic acid, and thiols: implications for uncoupling endothelial nitric-oxide synthase. *J Biol Chem.* 2003;278:22546–22554.
21. Vasquez-Vivar J, Martasek P, Whittsett J, Joseph J, Kalyanaraman B. The ratio between tetrahydrobiopterin and oxidized tetrahydrobiopterin analogues controls superoxide release from endothelial nitric oxide synthase: an EPR spin trapping study. *Biochem J.* 2002;362:733–739.
22. Vasquez-Vivar J, Martasek P, Kalyanaraman B. Superoxide generation from nitric oxide synthase: role of cofactors and protein interaction. In: *Biological Magnetic Resonance*. Boston, Mass: Kluwer Academic Publishers; 2005:75–91.
23. Rodriguez-Crespo I, Gerber NC, Ortiz de Montellano PR. Endothelial nitric-oxide synthase. Expression in *Escherichia coli*, spectroscopic characterization, and role of tetrahydrobiopterin in dimer formation. *J Biol Chem.* 1996;271:11462–11467.
24. Alp NJ, Mussa S, Khoo J, Guzik TJ, Cai S, Jefferson A, Rockett KA, Channon KM. Tetrahydrobiopterin-dependent preservation of nitric oxide-mediated endothelial function in diabetes by targeted transgenic GTP-cyclohydrolase I overexpression. *J Clin Invest.* 2003;112:725–735.
25. Ohashi Y, Kawashima S, Hirata K, Yamashita T, Ishida T, Inoue N, Sakoda T, Kurihara H, Yazaki Y, Yokoyama M. Hypotension and reduced nitric oxide-elicited vasorelaxation in transgenic mice overexpressing endothelial nitric oxide synthase. *J Clin Invest.* 1998;102:2061–2071.
26. Alp NJ, McAteer MA, Khoo J, Choudhury RP, Channon KM. Increased endothelial tetrahydrobiopterin synthesis by targeted transgenic GTP-cyclohydrolase I overexpression reduces endothelial dysfunction and atherosclerosis in ApoE-knockout mice. *Arterioscler Thromb Vasc Biol.* 2004;24:445–450.
27. Klatt P, Schmidt K, Lehner D, Glatter O, Bachinger HP, Mayer B. Structural analysis of porcine brain nitric oxide synthase reveals a role for tetrahydrobiopterin and L-arginine in the formation of an SDS-resistant dimer. *EMBO J.* 1995;14:3687–3695.
28. Cai S, Alp NJ, Mc Donald D, Canevari L, Heales S, Channon KM. GTP cyclohydrolase I gene transfer augments intracellular tetrahydrobiopterin in human endothelial cells: effects on nitric oxide synthase activity, protein levels and dimerization. *Cardiovasc Res.* 2002;55:838–849.
29. Rockett KA, Brookes R, Udalova I, Vidal V, Hill AV, Kwiatkowski D. 1,25-Dihydroxyvitamin D3 induces nitric oxide synthase and suppresses growth of *Mycobacterium tuberculosis* in a human macrophage-like cell line. *Infect Immun.* 1998;66:5314–5321.
30. Kleschyov AL, Munzel T. Advanced spin trapping of vascular nitric oxide using colloid iron diethyldithiocarbamate. *Methods Enzymol.* 2002;359:42–51.
31. Bendall JK, Heymes C, Wright TJ, Wheatcroft S, Grieve DJ, Shah AM, Cave AC. Strain-dependent variation in vascular responses to nitric oxide in the isolated murine heart. *J Mol Cell Cardiol.* 2002;34:1325–1333.
32. Skatchkov MP, Sperling D, Hink U, Mulsch A, Harrison DG, Sindermann I, Meinertz T, Munzel T. Validation of lucigenin as a chemiluminescent probe to monitor vascular superoxide as well as basal vascular nitric oxide production. *Biochem Biophys Res Commun.* 1999;254:319–324.
33. Khan SA, Lee K, Minhas KM, Gonzalez DR, Raju SVY, Tejani AD, Li D, Berkowitz DE, Hare JM. Neuronal nitric oxide synthase negatively regulates xanthine oxidoreductase inhibition of cardiac excitation-contraction coupling. *Proc Natl Acad Sci U S A.* 2004;101:15944–15948.
34. Channon KM, Qian HS, Neplioeva V, Blazing MA, Olmez E, Shetty GA, Youngblood SA, Stamler JS, George SE. In vivo gene transfer of nitric oxide synthase enhances vasomotor function in carotid arteries from normal and cholesterol-fed rabbits. *Circulation.* 1998;98:1905–1911.
35. Kawashima S, Yamashita T, Ozaki M, Ohashi Y, Azumi H, Inoue N, Hirata K-i, Hayashi Y, Itoh H, Yokoyama M. Endothelial NO synthase overexpression inhibits lesion formation in mouse model of vascular remodeling. *Arterioscler Thromb Vasc Biol.* 2001;21:201–207.
36. Tzeng E, Billiar TR, Robbins PD, Loftus M, Stuehr DJ. Expression of human inducible nitric oxide synthase in a tetrahydrobiopterin (H4B)-deficient cell line—H4B promotes assembly of enzyme subunits into an active enzyme. *Proc Natl Acad Sci U S A.* 1995;92:11771–11775.
37. Wever RMF, van Dam T, van Rijn HJ, de Groot F, Rabelink TJ. Tetrahydrobiopterin regulates superoxide and nitric oxide generation by recombinant endothelial nitric oxide synthase. *Biochem Biophys Res Commun.* 1997;237:340–344.

# Circulation

JOURNAL OF THE AMERICAN HEART ASSOCIATION

American Heart  
Association®   
*Learn and Live<sup>SM</sup>*

## **Possible Role of Brain-Derived Neurotrophic Factor in the Pathogenesis of Coronary Artery Disease**

Junya Ejiri, Nobutaka Inoue, Seiichi Kobayashi, Rio Shiraki, Kazunori Otsui,  
Tomoyuki Honjo, Motonori Takahashi, Yoshitaka Ohashi, Shinobu Ichikawa,  
Mitsuyasu Terashima, Takao Mori, Kojiro Awano, Toshiro Shinke, Junya Shite,  
Ken-ichi Hirata, Hiroshi Yokozaki, Seinosuke Kawashima and Mitsuhiro Yokoyama  
*Circulation* 2005;112;2114-2120; originally published online Sep 26, 2005;

DOI: 10.1161/CIRCULATIONAHA.104.476903

Circulation is published by the American Heart Association, 7272 Greenville Avenue, Dallas, TX  
72514

Copyright © 2005 American Heart Association. All rights reserved. Print ISSN: 0009-7322. Online  
ISSN: 1524-4539

The online version of this article, along with updated information and services, is  
located on the World Wide Web at:

<http://circ.ahajournals.org/cgi/content/full/112/14/2114>

Subscriptions: Information about subscribing to *Circulation* is online at  
<http://circ.ahajournals.org/subscriptions/>

Permissions: Permissions & Rights Desk, Lippincott Williams & Wilkins, a division of Wolters  
Kluwer Health, 351 West Camden Street, Baltimore, MD 21202-2436. Phone: 410-528-4050. Fax:  
410-528-8550. E-mail:  
[journalpermissions@lww.com](mailto:journalpermissions@lww.com)

Reprints: Information about reprints can be found online at  
<http://www.lww.com/reprints>

# Possible Role of Brain-Derived Neurotrophic Factor in the Pathogenesis of Coronary Artery Disease

Junya Ejiri, MD, PhD; Nobutaka Inoue, MD, PhD; Seiichi Kobayashi, MD, PhD; Rio Shiraki, MD; Kazunori Otsui, MD; Tomoyuki Honjo, MD; Motonori Takahashi, MD; Yoshitaka Ohashi, MD, PhD; Shinobu Ichikawa, MD, PhD; Mitsuyasu Terashima, MD; Takao Mori, MD, PhD; Kojiro Awano, MD, PhD; Toshiro Shinke, MD, PhD; Junya Shite, MD, PhD; Ken-ichi Hirata, MD, PhD; Hiroshi Yokozaki, MD, PhD; Seinosuke Kawashima, MD, PhD; Mitsuhiro Yokoyama, MD, PhD

**Background**—The neurotrophin (NT) family, including nerve growth factor NT-3 and brain-derived neurotrophic factor (BDNF), has a critical role in the survival, growth, maintenance, and death of central and peripheral neurons. NTs and their receptors are expressed in atherosclerotic lesions; however, their significance in cardiovascular disease remains unclear.

**Methods and Results**—To clarify the role of NTs in the pathogenesis of coronary artery disease, NT plasma levels in the aorta, coronary sinus, and peripheral veins of patients with unstable angina (n=38), stable effort angina (n=45), and non-coronary artery disease (n=24) were examined. In addition, regional expression of BDNF in coronary arteries was examined in autopsy cases and patients with angina pectoris by directional coronary atherectomy. The difference in BDNF levels, but not NT-3, between the coronary sinus and aorta was significantly greater in the unstable angina group compared with the stable effort angina and non-coronary artery disease groups. Immunohistochemical investigations demonstrated BDNF expression in the atheromatous intima and adventitia in atherosclerotic coronary arteries. BDNF expression was enhanced in macrophages and smooth muscle cells in atherosclerotic coronary arteries. Stimulation with recombinant BDNF significantly enhanced NAD(P)H oxidase activity and the generation of reactive oxygen species in cultured human coronary artery smooth muscle cells.

**Conclusions**—BDNF has an important role in atherogenesis and plaque instability via the activation of NAD(P)H oxidase. (*Circulation*. 2005;112:2114-2120.)

**Key Words:** circulation ■ coronary disease ■ free radicals ■ nervous system ■ stress

On January 17, 1995, the great Hanshin-Awaji earthquake hit Kobe, Japan, killing 6433 people. Thereafter, there was an increase in mortality from cardiac disease.<sup>1</sup> Chronic psychological stress appears to have an important role in cardiovascular diseases after traumatic events such as a major earthquake.<sup>2</sup> Psychological factors such as depression and acute and chronic stress are potent risk factors for coronary artery disease (CAD).<sup>2</sup> The precise mechanisms by which psychological factors cause cardiovascular disease, however, remain to be determined. Under psychological stress, the hypothalamus-pituitary-adrenal axis and sympathetic nerve system are activated, and a wide range of neurohumoral factors are dynamically regulated, including neurotrophins (NTs).

NTs form a family of dimeric polypeptides, which include nerve growth factor, brain-derived neurotrophic factor (BDNF), NT-3, and NT-4/5 in humans.<sup>3-5</sup> NTs have critical

roles in the survival, growth, maintenance, and death of central and peripheral neurons.<sup>5,6</sup> Under psychological stress, the secretion of NTs from the hypothalamus, pituitary gland, and central and peripheral nerves is markedly altered.<sup>7</sup> The biological activities of NTs are mediated via the specific high-affinity receptors trkA, trkB, and trkC and the low-affinity NT receptor p75.<sup>8,9</sup> NTs and their receptors are expressed in nonneuronal tissues and various cell types such as developing heart,<sup>10</sup> spleen,<sup>11</sup> atherosclerotic vessels,<sup>12</sup> macrophages,<sup>13</sup> lymphocytes,<sup>14</sup> endothelial cells,<sup>15</sup> and vascular smooth muscle cells,<sup>12</sup> suggesting that NTs have diverse roles even in nonneural organs. The significance of NTs in cardiovascular disease remains to be elucidated.

Acute coronary syndrome occurs as a consequence of coronary plaque rupture and superimposed thrombus. Reactive oxygen species derived from NAD(P)H oxidase have a critical role in the pathogenesis of CAD and plaque instabil-

Received May 21, 2004; revision received May 10, 2005; accepted July 15, 2005.

From the Division of Cardiovascular and Respiratory Medicine, Department of Internal Medicine (J.E., N.I., S.K., R.S., K.O., T.H., M.T., T.S., J.S., K.H., S.K., M.Y.), and Division of Surgical Pathology, Department of Biological Informatics, Kobe University Graduate School of Medicine (H.Y.), and Division of Cardiology, Miki City Hospital (Y.O., S.I., M.T., T.M., K.A.), Kobe, Japan.

Correspondence to Nobutaka Inoue, MD, PhD, Division of Cardiovascular and Respiratory Medicine, Department of Internal Medicine, Kobe University Graduate School of Medicine, 7-5-2, Kusunoki-cho, Chuo-ku, Kobe 650-0017, Japan. E-mail nobutaka@med.kobe-u.ac.jp

© 2005 American Heart Association, Inc.

*Circulation* is available at <http://www.circulationaha.org>

DOI: 10.1161/CIRCULATIONAHA.104.476903